

UNCLASSIFIED

AD NUMBER	
AD348497	
CLASSIFICATION CHANGES	
TO:	UNCLASSIFIED
FROM:	CONFIDENTIAL
LIMITATION CHANGES	
TO: Approved for public release; distribution is unlimited.	
FROM: Distribution authorized to U.S. Gov't. agencies and their contractors; Administrative/Operational Use; 11 OCT 1963. Other requests shall be referred to Aeronautical Systems Div., Det. 4, Eglin AFB, FL.	
AUTHORITY	
31 Jan 1976, DoDD 5200.10 ; ASD ltr 30 May 1973	

THIS PAGE IS UNCLASSIFIED

UNCLASSIFIED

AD

348497

DEFENSE DOCUMENTATION CENTER

FOR

SCIENTIFIC AND TECHNICAL INFORMATION

CAMERON STATION, ALEXANDRIA, VIRGINIA



UNCLASSIFIED

NOTICE: When government or other drawings, specifications or other data are used for any purpose other than in connection with a definitely related government procurement operation, the U. S. Government thereby incurs no responsibility, nor any obligation whatsoever; and the fact that the Government may have formulated, furnished, or in any way supplied the said drawings, specifications, or other data is not to be regarded by implication or otherwise as in any manner licensing the holder or any other person or corporation, or conveying any rights or permission to manufacture, use or sell any patented invention that may in any way be related thereto.

NOTICE:

THIS DOCUMENT CONTAINS INFORMATION  
AFFECTING THE NATIONAL DEFENSE OF  
THE UNITED STATES WITHIN THE MEAN-  
ING OF THE ESPIONAGE LAWS, TITLE 18,  
U.S.C., SECTIONS 793 and 794. THE  
TRANSMISSION OR THE REVELATION OF  
ITS CONTENTS IN ANY MANNER TO AN  
UNAUTHORIZED PERSON IS PROHIBITED  
BY LAW.

348497

CATALOGED BY DDC

AS AD No. 1

ASD-TDR-64-3

~~CONFIDENTIAL~~

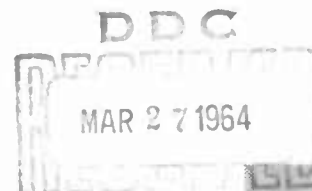
Copy No. 85 of 205 Copies

(UNCLASSIFIED TITLE)

● **Impact Failure of Pressure  
Vessels - Part 2**

11 October 1963

**ASD Technical Documentary Report No. ASD-TDR-64-3  
JANUARY 1964 • AFSC Projects 9850, 2835**



DIRECTORATE OF ARMAMENT DEVELOPMENT  
**Det 4, AERONAUTICAL SYSTEMS DIVISION**  
AIR FORCE SYSTEMS COMMAND • UNITED STATES AIR FORCE

**EGLIN AIR FORCE BASE, FLORIDA**

(Prepared under Contract AF08(635)-2889 by Aero-Space Division,  
The Boeing Company, Seattle, Washington. Authors: G. T. Burch, Jr.,  
D. H. Lee, J. F. Lundberg)



GROUP-4  
Downgraded at 3 year intervals;  
Declassified after 12 years.

~~CONFIDENTIAL~~

348497



Qualified requesters may obtain copies from DDC. Orders will be expedited if placed through the librarian or other person designated to request documents from DDC.

This document contains information affecting the national defense of the United States within the meaning of the Espionage Laws (Title 18, U.S.C., sections 793 and 794). Transmission or revelation in any manner to an unauthorized person is prohibited by law.

When US Government drawings, specifications, or other data are used for any purpose other than a definitely related government procurement operation, the government thereby incurs no responsibility nor any obligation whatsoever; and the fact that the government may have formulated, furnished, or in any way supplied the said drawings, specifications, or other data is not to be regarded by implication or otherwise, as in any manner licensing the holder or any other person or corporation, or conveying any rights or permission to manufacture, use, or sell any patented invention that may in any way be related thereto.

DDC release to OTS is not authorized.

Copies of this report should not be returned to the Aeronautical Systems Division unless return is required by security considerations, contractual obligations, or notice on a specific document.

#### KEYWORD LIST

Listed below are keywords which serve as an index to the contents of this report (AFR 80-29).

Pressure vessels  
Impact shock  
Stresses  
Structural shells  
Fracture (mechanics)

**CONFIDENTIAL****ABSTRACT**

The objective of this program is to provide a means for predicting the conditions under which a pressure vessel will fail due to hypervelocity impact. A major segment of the experimental portion of the program has been accomplished. The data show that a preimpact stress field does not affect hypervelocity cratering or penetration, but the conditions for catastrophic fracture depend on both the stress field and the hole size. A correlating factor between the preimpact stress and the hole size has been established. Systematic test series of shielded structural arrangements have been performed to investigate projectile dispersion, cratering characteristics, impact damage, and failure modes. Interrelationships between projectile geometry, specimen size, material, and structural damage have been observed. In addition, tests have shown that the limiting conditions for catastrophic fracture of gas- and liquid-filled pressure vessels differ from each other; further investigations are needed, especially to determine failure conditions for liquid-filled vessels.

**PUBLICATION REVIEW**

THIS TECHNICAL DOCUMENTARY REPORT HAS BEEN  
REVIEWED AND IS APPROVED.

  
BEN F. HARDAWAY Lt. Col.  
COLONEL, USAF  
CHIEF, WEAPONS DIVISION

**CONFIDENTIAL**

## CONTENTS

	<u>Page</u>
I. SUMMARY	1
II. INTRODUCTION	2
III. THE EXPERIMENTAL PROGRAM	3
Phase I — Fracture Mechanics	3
Phase II — Stressed Sheet	3
Phase III — Projectile Geometry	3
Phase IV — Pressure Vessels	3
IV. PHASE I TEST RESULTS	4
0.100-Inch 7075-T6 Specimens	5
0.400-Inch 7075-T6 Specimens	11
0.900-Inch 7075-T6 Specimens	15
Ladish D6AC Specimens	15
V. PHASE II TEST RESULTS	18
Single Sheet Specimens	18
Shielded Specimens	21
Fractures	32
Insulation Fillers	39
Backing Media	39
VI. PHASE III TEST RESULTS	45
VII. PHASE IV TEST RESULTS	54
Unshielded Air-Pressurized Tanks	54
Shielded Air-Pressurized Tanks	54
Water-Filled Tanks	59
VIII. CONCLUSIONS	63
IX. REFERENCES	65

## ILLUSTRATIONS

		<u>Page</u>
1	Test Specimens and Loading Frame	7
2	Fracture Mechanics Tests — 0.100-Inch 7075-T6 Specimens	8
3	Fracture Strength of 0.100-Inch 7075-T6 Specimens	9
4	Fracture Mechanics Tests — Effect of Shields	10
5	Fracture Mechanics Tests — Effect of Specimen Width	12
6	Fracture Mechanics Tests — 0.400-Inch 7075-T6 Specimens	13
7	Fracture Strength of 0.400-Inch 7075-T6 Specimens	14
8	Fracture Mechanics Tests — 0.900-Inch 7075-T6 Specimens	16
9	Fracture Mechanics Tests — 0.250-Inch Ladish D6AC Specimens	17
10	Effect of Target Stress on Hole Size	22
11	Effect of Static Stress on Unshielded Specimens	23
12	Effect of Target Thickness on Hole Size	24
13	Effect of Target Thickness on Impact Damage	25
14	Projectile and Target Scaling — Craters	26
15	Projectile and Target Scaling — Penetrations	27
16	Effect of Shield Thickness — 1/4-Inch Projectile	29
17	Effect of Shield Thickness — 1/8-Inch Projectile	30
18	Shielded Specimen Damage Versus Shield Thickness	31
19	Effect of Static Stress on Shielded Specimens	33
20	Fracture Strength of 0.090-Inch 2014-T6 Specimens	34
21	Damage Due to Impact of 1/8-Inch Projectile Plus Sabot	36
22	Large Deflection Impact Damage	37
23	Effect of Specimen Width on Large Deflection Impact Damage	38
24	Effect of 2-Inches of Q-Felt Insulation Filler	40
25	Effect of Paraffin Backing on Impact Damage — 1/8-Inch Projectile	42
26	Effect of Paraffin Backing on Impact Damage — 1/4-Inch Projectile	43
27	Damage to Paraffin Backing Blocks After Penetration of 0.090-Inch 2014-T6 Specimens	44
28	Projectile Geometry	46

	<u>Page</u>
29     Projectiles in Flight	48
30     Effect of Projectile Geometry — Craters in Unshielded Specimens	49
31     Effect of Projectile Geometry — Penetrations in Unshielded Specimens	50
32     Effect of Projectile Geometry and Shield Thickness	51
33     Comparison of Unshielded Tests of Uniaxial and Biaxial Specimens	56
34     Light-Gas Gun Range and Tank Specimen	57
35     Comparison of Shielded Tests of Uniaxial and Biaxial Specimens	58
36     Impact Damage of Unshielded, Water-Filled Tanks	61
37     Impact Damage of Shielded, Water-Filled Tanks	62

#### TABLES

1     Phase I Tests	6
2     Phase II Tests	19
3     Phase III Tests	47
4     Phase IV Tests	55

## **CONFIDENTIAL**

### **I. SUMMARY**

The impact failure of space vehicles is, in large measure, defined by the impact failure of pressure vessels. An experimental program has been designed to develop data on impact failure conditions for pressure vessels. A major segment of the testing has been accomplished. Test phases have investigated the applicability of fracture mechanics concepts to hypervelocity impact, and the effect of specimen and projectile geometry on the impact damage to practical structural configurations.

The hypervelocity impact tests of stressed specimens have shown that an analytical relationship exists between a limiting preimpact stress and a critical hole size. This relationship has been correlated in terms of fracture toughness values analogous to those of static fracture mechanics. Several generic types of fracture toughness values characteristic of hypervelocity impact have been distinguished applicable to thin-sheet penetration, to thick-sheet cratering and penetration, or to penetration accompanied by major deformation around the hole. This latter is typical of impact damage to heavily shielded structures.

Impact tests of specimens preloaded to various stress levels have shown that the cratering and penetration are independent of stress, but are dependent in a complex manner on shielding arrangements and projectile geometry. Under certain circumstances a simple penetration can be transformed to catastrophic fracture by the addition of a shield or by a change in projectile geometry. Impact into liquid-filled pressure vessels produces a pressure pulse that may induce catastrophic fracture; more work is required to determine the limiting magnitude of pulse and the associated impact damage required for fracture under these circumstances.

## II. INTRODUCTION

Survivability in space, for both manned and unmanned space vehicles, is a subject of increasing concern as the scope and tempo of space programs increase. Space vehicles are, typically, accumulations of pressure vessels of various sizes and shapes designed to house or support different vehicles. A major consideration in assessment of survivability is the damage caused by the impact of hypervelocity particles. The amount, the type, and the significance of the damage depend on the characteristics of the particle, on the structural configuration, and on the mission requirements.

The vulnerability of space vehicles is, in large measure, the vulnerability of pressure vessels. The objective of this program is to determine pressure-vessel failure modes due to hypervelocity impact, and to provide a means for predicting conditions of failure. To accomplish this, a search has been made for impact theories and data on the failure of loaded structure. The results of the literature search have been reported in Reference 1. Although many impact studies have been performed, little that is directly applicable to pressure-vessel failure modes has been published. No adequate theory of hypervelocity penetration and structural response is available. A major reliance, then, for evaluating failure modes has devolved upon experimental studies. In this program, experimental studies have been designed to determine the effect of particle impact on stressed specimens representative of pressure-vessel structural materials and configurations.

The phenomenological aspects of impact into realistic structural arrangements are manifold, complex, and poorly defined. A testing program designed to investigate pressure-vessel failure by varying all identifiable factors is grossly impractical in size. A new concept of impact failure is needed to determine the parameters significant in describing impact failure. Fracture mechanics, relating stress fields to material flaws, has been found useful in predicting static and fatigue failures. It is reasonable to postulate that an analogous relation exists between a limiting preimpact stress and hypervelocity crater size. The development of this concept for a reasonable range of projectile, material, and geometric variables has formed the central theme of the experimental program. A major segment of the testing has been accomplished. A description of the tests and an evaluation of the data are contained in this report.

## **CONFIDENTIAL**

### **III. THE EXPERIMENTAL PROGRAM**

The concept of the experimental program is based on physical insight into penetration mechanics and the concomitant structural response, formulated in a four-phase test series. These phases are defined as follows:

#### **Phase I-Fracture Mechanics**

Failures of structures at stresses far below their design values have motivated extensive research into fracture phenomena. The Griffith-Irwin approach to fracture mechanics has been used with considerable success in predicting fracture behavior. The Phase I tests of this program have been designed to investigate the applicability of fracture mechanics to hypervelocity impact. Two brittle materials, 7075-T6 aluminum and Ladish D6AC steel, have been selected so that the critical crack lengths and the test impact craters are of comparable size.

#### **Phase II-Stressed Sheet**

Little is known about the effect of hypervelocity impact on practical structural materials and configurations. It is the purpose of Phase II testing to investigate impact and penetration effects on such configurations. These tests have been designed to determine possible coupling between static stress and hypervelocity impact phenomena. Stressed 2014-T6 aluminum sheet has been tested with and without shielding. The effect of placing a low-density insulation-type filler between the shield and the stressed specimen has also been investigated. The effect of propellants on tank structural response due to hypervelocity impact has been simulated by placing suitable backing material against the stressed specimen.

#### **Phase III-Projectile Geometry**

Phase III tests have been designed to investigate the effect of projectile geometry on penetration characteristics of shielded and unshielded stressed specimens. Target material has been 2014-T6 aluminum. Emphasis has been on those projectile shapes that are not sensitively dependent on impact attitude. The projectiles that have been successfully launched are spheres, hollow cylinders, equilateral tetrahedrons, and cupped cubes.

#### **Phase IV-Pressure Vessels**

Phase IV consists of tests of 2014-T6 spherical, water-filled tanks and air-pressurized tanks with and without shielding. Tanks of two diameters have been tested in order to provide some information on the possible effects of curvature on failure. These test series have been designed to provide confirmation of the results obtained from previous testing and to provide a correlation between uniaxial and biaxial stress systems.



## CONFIDENTIAL

### IV. PHASE I TEST RESULTS

The phenomena of structural failures at average stresses far below their design values have been investigated intensely in the past few years. Among the methods proposed for prediction of these failures, the Griffith-Irwin approach to fracture mechanics has met with considerable success in describing static and fatigue fractures. The Griffith-Irwin theory assumes a relatively slow application of load and the existence of sharp cracks or flaws in the material. A stress intensity factor,  $K$ , represents the combined effect of material properties, the crack dimensions, and the stress field, all of which influence the subsequent behavior of the crack. The critical value of  $K$ , corresponding to the onset of rapid crack growth, is expressed as the fracture toughness value,  $K_C$ . The essential thesis is that, for a material having a given value of  $K_C$ , rapid crack propagation will ensue whenever the stress-intensity factor of the stress field surrounding a crack surpasses the value of  $K_C$ .

In recent years, fracture toughness testing has been undertaken by various organizations. Several test procedures have been evolved, and several criteria for evaluating materials in terms of fracture toughness have been suggested. The difficulties involved are still far from resolution. It has been demonstrated that the fracture toughness value is a function of many variables, including material, specimen width and thickness, ambient temperature, material heat-treat, and the type of test. Test results have shown that it is possible for the same material to be interpreted to have either low or high fracture toughness, depending on the details of the tests (References 2 and 3). In addition, uncertainties exist in the relationship between fractures in actual structures and in  $K_C$  test specimens. Environmental, dimensional, and crack-shape parameters for the service-incurred fracture are not the same as for the  $K_C$  test. Because of these differences, the apparent  $K_C$  applicable to the fracture of structures may differ from the value of  $K_C$  measured by a standard laboratory test procedure (Reference 4).

The types of fracture and the accompanying fracture toughness values can be divided into two characteristic groups. Thin specimens allow shear-type, or plane-stress, fracture at relatively high fracture toughness values. Thick specimens provide elastic constraint along the crack tip producing plane-strain fracture at low fracture toughness values. The plane-stress fracture toughness is denoted by  $K_C$  while plane-strain fracture toughness values are designated as  $K_{Ic}$ .

Although the flaw shape and conditions of loading under hypervelocity impact do not fulfill the analytical conditions of fracture mechanics, it is reasonable to expect that a limiting stress as a function of crater size should exist. Phase I tests have been designed to determine whether the established technology of fracture mechanics can be utilized to describe hypervelocity impact failure modes. Materials of distinctly different metallurgical structure (i.e., 7075-T6 aluminum and Ladish D6AC steel) have been tested in several thicknesses to investigate

## CONFIDENTIAL

both plane-strain and plane-stress failure modes. The test data are listed in Table 1. Discussions of the several series of Phase I tests follow.

### 0.100-Inch 7075-T6 Specimens

Static fracture toughness tests have shown that 7075-T6 aluminum can fail at stresses much lower than yield stress in both plane-stress and plane strain failure modes. These static data indicate that a 0.100-inch specimen will fail in plane-stress. The first hypervelocity test series was of 0.100-inch specimens to determine if failures under hypervelocity impact would also be plane-stress or if impact would induce plane-strain failures at lower static loadings.

The test specimen used for these tests was a 5-inch wide tensile coupon. Figure 1 shows typical specimens, the loading jig, and the hypervelocity testing range. Projectiles were 1/4-inch diameter aluminum cylinders with a mass of 0.54 gram; velocities were about 15,000 feet per second. These pellets produced holes about 0.60 inch in diameter. No failures were obtained at 60,000 psi, but when the static stress was increased to 65,000 psi, the specimen fractured during impact. Photographs of these tests are shown in Figure 2. Figure 3, a plot of gross stress versus hole diameter, indicates a static fracture toughness value of about  $60 \text{ ksi} \sqrt{\text{in}}$ . These tests were repeated using 1/4-inch diameter Lexan (a polycarbonate) cylinders. The 0.23-gram Lexan projectiles produced 0.67-inch holes at velocities of 24,000 feet per second. One specimen, initially stressed to 58,700 psi, sustained impact without fracture but failed when a slight increase of stress was applied while the specimen was being removed from the test jig. This coincides with the  $60 \text{ ksi} \sqrt{\text{in}}$  value of the first tests. A photograph of this test is shown in Figure 4a.

To show that fracture mechanics concepts apply to hypervelocity impact, holes of different sizes are required. Smaller holes would require higher stresses approaching the yield strength of the material. Larger holes require larger projectiles, a physical impossibility for the testing facilities. An alternate approach would be to use a thin shield to break up the projectile, spreading the damaging particles over a larger area and producing a larger hole. This method was followed. A standard 5-inch wide stressed specimen was shielded with a 0.020-inch sheet spaced 2 inches in front. A 1/4-inch diameter aluminum sphere of 0.38-gram mass impacting this combination target at 18,000 feet per second produced a 1-inch diameter hole in the stressed specimen. Photographs of typical shielded tests are shown in Figure 4. A test series using shielded targets preloaded to various static stresses indicated a fracture toughness value of 40 to 45  $\text{ksi} \sqrt{\text{in}}$ . While this does not agree with the value obtained by the unshielded tests, a standard, center-crack static fracture toughness test using a 5-inch wide specimen cut from the same sheet of material produced a value of 44.4  $\text{ksi} \sqrt{\text{in}}$ . The critical crack length for the static test was 1.013 inches. Both the shielded test data and the static fracture toughness test value are shown in Figure 3.

CONFIDENTIAL

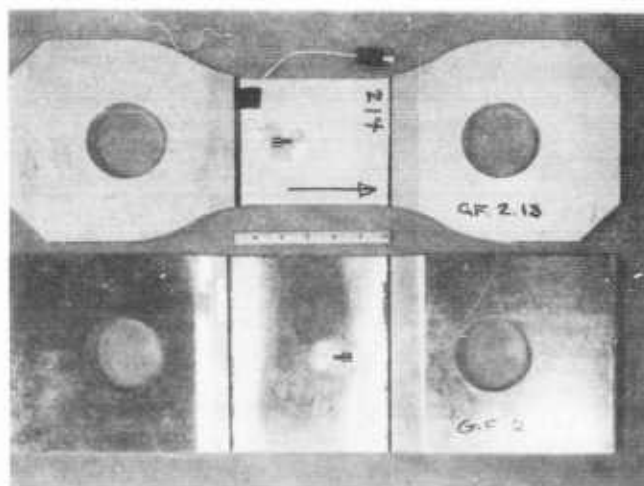
Test No.	STRESSED SPECIMEN				SHIELD			Type	PROJECTILE			FIG NO.	NOTES
	Width & Thick. (inches)	Matl	Stress (psi)	Crater Dia (inches)	Damage Dia (inches)	Failure Mode	Thick. (inches)	Matl	Spacing (inches)	Filler	Hole Dia (inches)		
T-29	5 .100	7075-T6	60,000	P .51		NF							
T-30	5 .100	7075-T6	65,500	P .60		F							
T-217	5 .097	7075-T6	58,700	P .67		FR							
T-218	5 .097	7075-T6	58,200	P 1.10	1.60	F	.020	7075-T6	2		.29		
T-219	5 .097	7075-T6	40,300	P 1.00	1.20	F	.020	7075-T6	2		.29		
T-222	5 .097	7075-T6	30,300	P 1.00	1.30	NF	.020	7075-T6	2		.29		
T-223	5 .097	7075-T6	35,000	P 1.00	1.30	F	.020	7075-T6	2		.30		
T-314	8 .100	7075-T6	39,000	P 1.00	1.40	NF	.020	7075-T6	2		.32		
T-326	8 .100	7075-T6	50,500	P 1.05	1.40	NF	.020	7075-T6	2		.32		
T-315	8 .100	7075-T6	33,800	P .75	2.25	F	.250	2014-T6	2		.84		
T-36	4 .400	7075-T6	45,000	C .39		NF							
T-15	4 .400	7075-T6	21,000	P .55		NF							
T-16	4 .400	7075-T6	32,000	P .65		NF							
T-17	4 .400	7075-T6	39,000	P .59		NF							
R-8	4 .400	7075-T6	50,000	P .65		F							
R-19	4 .400	7075-T6	50,000	P .70		F							
T-96	4 .400	7075-T6	40,000	P .68		NF							
T-98	4 .400	7075-T6	50,600	P .76		F							
T-99	4 .400	7075-T6	45,700	P .78		F							
T-38	2.5 .900	7075-T6	41,000	C .41		NF							
T-41	2.5 .900	7075-T6	45,500	C .42		NF							
T-22	2.5 .895	7075-T6	30,300	C .72		NF							
T-23	2.5 .896	7075-T6	42,500	C .70		FR							
T-256	2.6 .250	Ladiuh	78,000	P .52		NF							
T-313	2.6 .250	Ladiuh	134,000	P .57		NF							
T-327	2.6 .250	Ladiuh	143,500	P .60		NF							
DML-1	1.5 .030	Ladiuh	90,000	P .03		NF							
DML-2	1.5 .250	Ladiuh	40,000	C .07		NF							

TABLE 1 - PHASE I TESTS

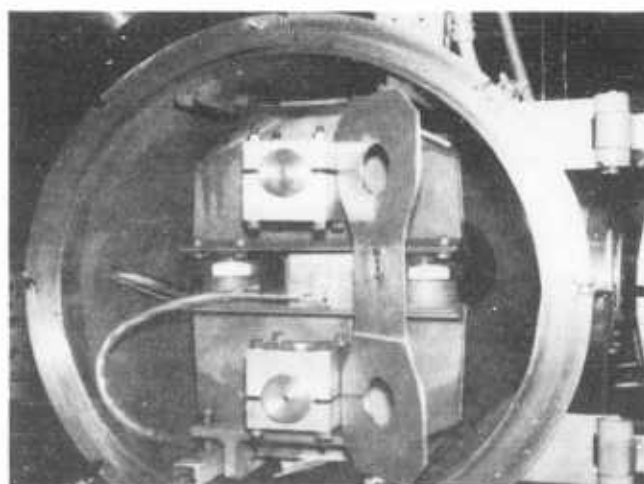
P = Complete Penetration  
 C = Crater, No Penetration  
 F = Specimen Fractured During Impact Event  
 NF = Specimen Did Not Fracture  
 FR = Specimen Fractured While Being Removed From the Jig  
 SP = Spherical Projectile

CY = Cylindrical Projectile  
 1 Specimen Shattered by Impact  
 2 Crater Too Far Off Center  
 3 No Velocity Measurement  
 4 Specimen Grain Improperly Oriented

CONFIDENTIAL



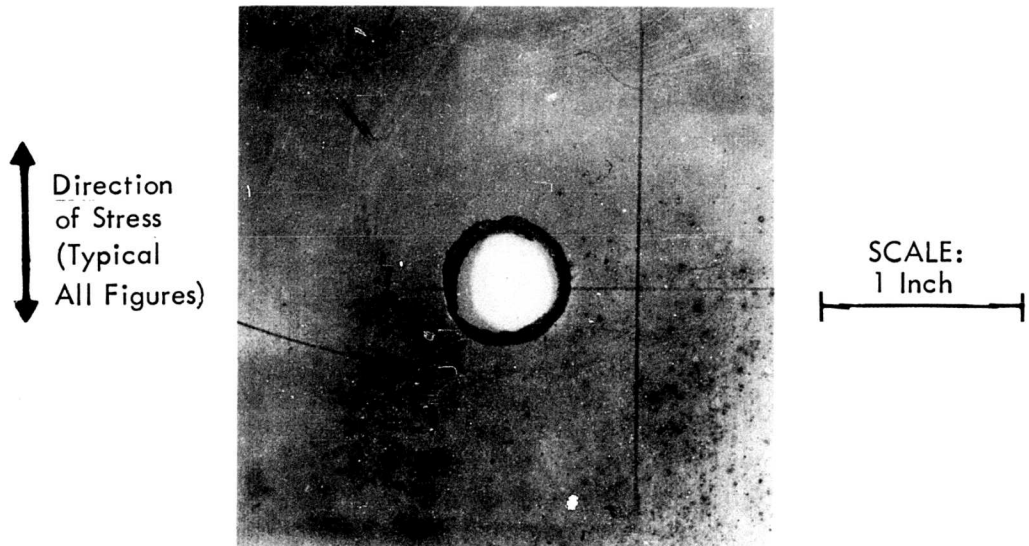
(a) Typical Test Specimens



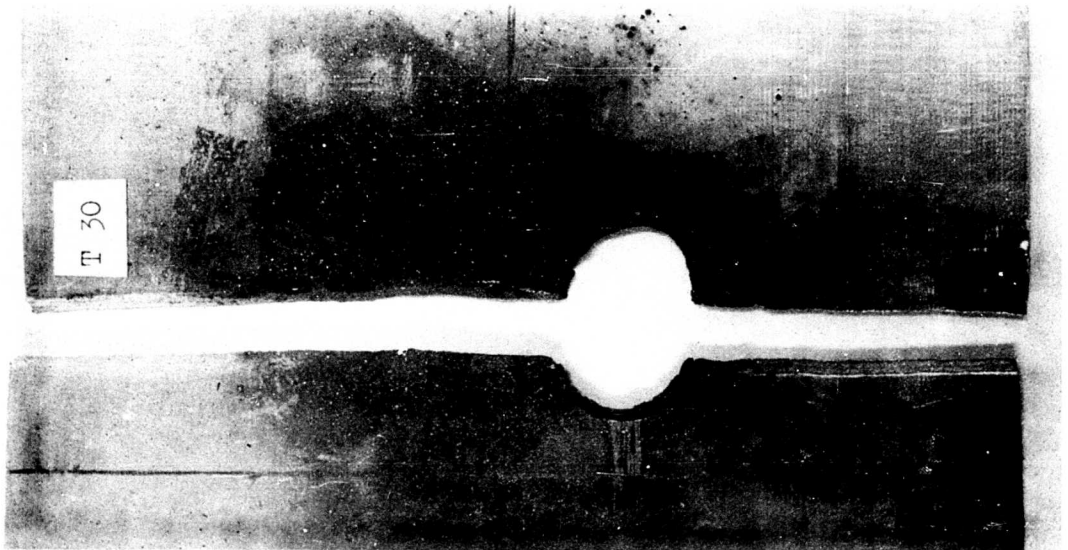
(b) Specimen and Loading Frame in Test Chamber

Figure 1 TEST SPECIMENS AND LOADING FRAME

**CONFIDENTIAL**



(a) Static Stress 60,000 psi

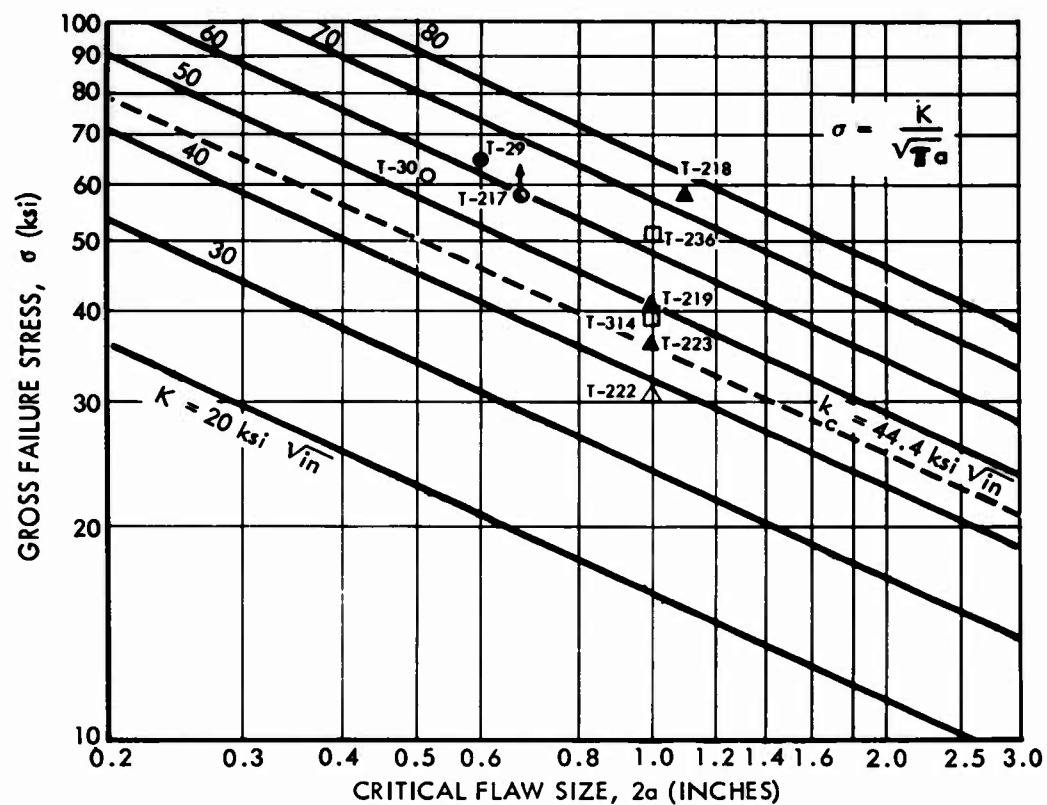


(b) Static Stress 65,500 psi

**Figure 2 FRACTURE MECHANICS TESTS -  
0.100-INCH 7075-T6 SPECIMENS  
1/4-Inch Aluminum Cylinder Projectiles**

**CONFIDENTIAL**

CONFIDENTIAL

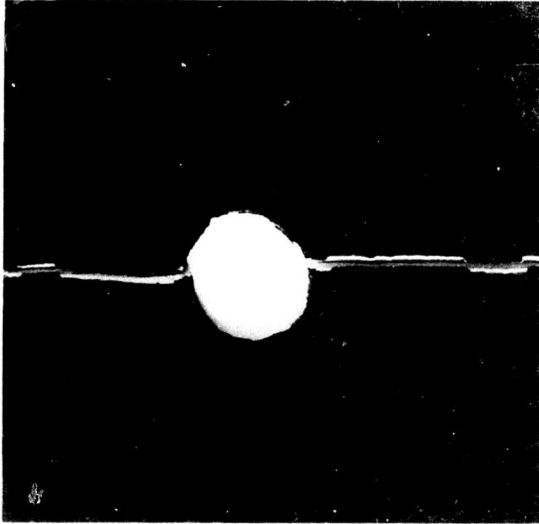


Fracture Occurred	No Fracture
●	○ 5-Inch Wide Specimen - No Shield
▲	△ 5-Inch Wide Specimen - 0.020-Inch Shield, 2-Inch Spacing
■	□ 8-Inch Wide Specimen - 0.020-Inch Shield, 2-Inch Spacing
●	Fracture Occurred During Removal From Jig

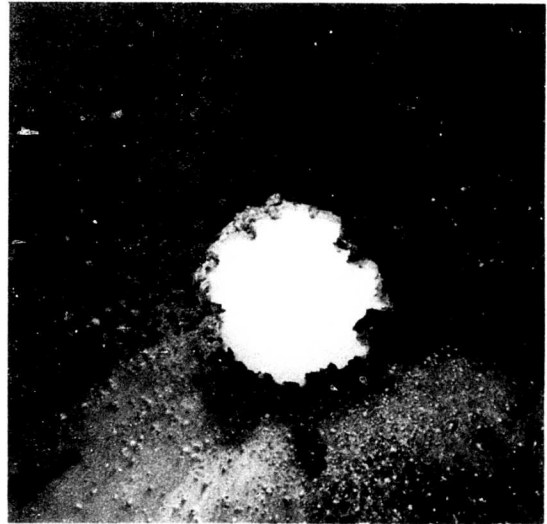
Figure 3 FRACTURE STRENGTH OF 0.100-INCH 7075-T6 SPECIMENS

CONFIDENTIAL

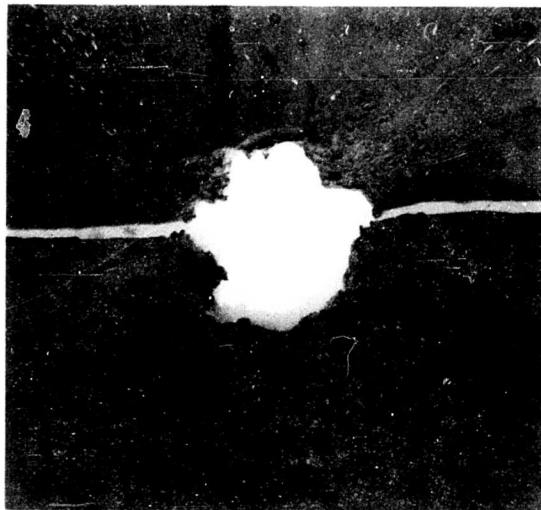
**CONFIDENTIAL**



(a) Unshielded Target  
Static Stress 58,700 psi



(b) 0.020-Inch Shield - 2-Inch Spacing  
Static Stress 30,300 psi



(c) 0.020-Inch Shield - 2-Inch Spacing  
Static Stress 35,000 psi

SCALE:  
1 Inch

**Figure 4 FRACTURE MECHANICS TESTS - EFFECT OF SHIELDS**

0.100-Inch 7075-T6 Specimens  
1/4-Inch Projectiles

**CONFIDENTIAL**

## CONFIDENTIAL

The inconsistency of the fracture toughness values obtained by the different configurations was suspected to be due to edge effects, especially for the shielded specimens. In order to investigate this problem, wider specimens were manufactured and tested. Tests performed using this new specimen have not failed at the same stress levels as did the 5-inch wide specimen. For example, the two tests shown in Figure 5 had the same nominal static stress, yet the 5-inch specimen fractured while the 8-inch specimen did not. A second specimen tested with a higher static stress also did not fail, indicating a minimum fracture toughness value of about  $60 \text{ ksi } \sqrt{\text{in.}}$ . This is consistent with the unshielded tests of 5-inch wide specimens. The hole-diameter-to-specimen-width ratio for the 8-inch wide shielded specimens is identical to that of the 5-inch wide unshielded specimens.

This series of tests has demonstrated that catastrophic fracture can occur during hypervelocity impact, even when the static stresses of the material are far below material ultimate strength. For example, in tests T219 and T-223, static gross stresses were 40,300 and 35,000 psi, respectively. Hypervelocity impact produced a 1.2-inch diameter hole. The net static stresses became, in turn, 53,000 and 46,000 psi. Those stresses are significantly below material yield strength.

All fractures of 0.100-inch specimens were plane-stress, with the failure surface inclined at about 45 degrees from the plane of the stressed sheet. This is the same as expected from static fracture considerations, hence hypervelocity impact did not change the mode of fracture.

### 0.400-Inch 7075-T6 Specimens

The 0.400-inch thick 7075-T6 specimens were chosen in an attempt to produce plane-strain failure modes with through-the-thickness flaws produced by the projectile penetration. This thickness is sufficiently thin to allow complete penetration, yet the thickness provides elastic constraint to the crack tip, preventing shear-type separation. The projectiles used to test these specimens were cylinders of aluminum and Lexan. Masses and impact velocities were 0.54 and 0.39 grams, and 15,000 and 23,000 feet per second, respectively. Photographs of typical tests of this series are shown in Figure 6. For the two tests shown in Figure 6, the net stresses were 55,000 psi for the unfractured test specimen and 60,000 psi for the fractured specimen. These values are below the nominal yield strength of 7075-T6.

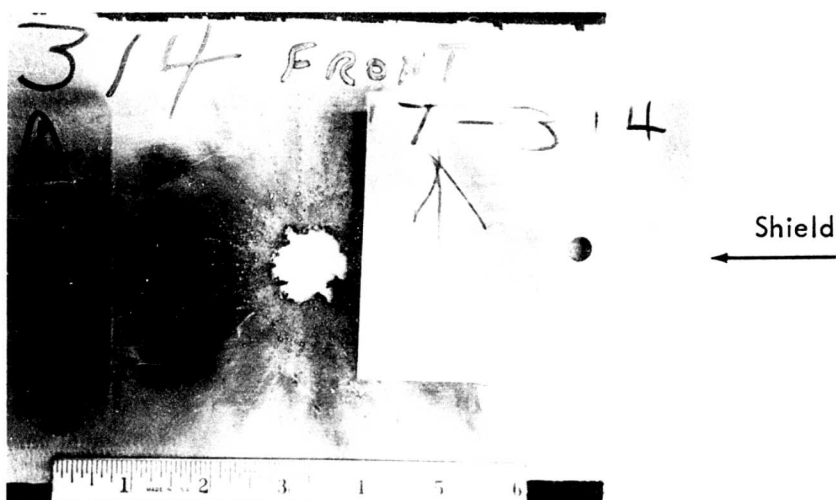
The results of the tests are plotted in Figure 7. All fractures shown in Figure 7 were plane-strain mode failures. A fracture toughness value between 40 and  $50 \text{ ksi } \sqrt{\text{in.}}$  is indicated. A center-crack static fracture toughness test was also performed on a specimen from the same material; a static fracture toughness value of  $27.5 \text{ ksi } \sqrt{\text{in.}}$  was obtained. This test series revealed that: (1) through-the-thickness plane-strain fracture will occur for 0.400-inch 7075-T6 aluminum specimens with net stresses far below their ultimate strength,



**CONFIDENTIAL**



(a) 5-Inch-Wide Specimen - Static Stress 40,300 psi



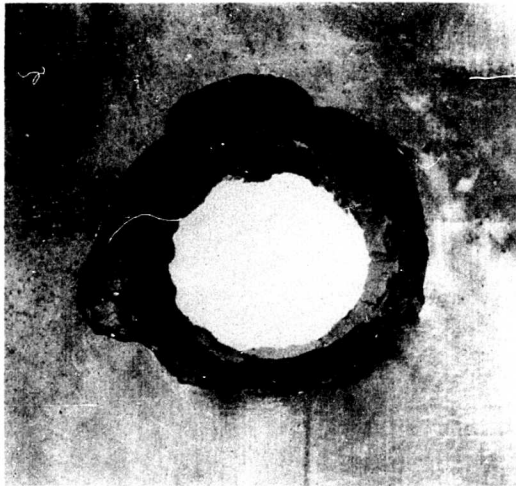
(b) 8-Inch-Wide Specimen — Static Stress 39,000 psi

## Figure 5 FRACTURE MECHANICS TESTS — EFFECT OF SPECIMEN WIDTH

0.100-Inch 7075-T6 Specimens  
1/4-Inch Aluminum Sphere Projectiles

**CONFIDENTIAL**

**CONFIDENTIAL**



(a) Entrance Side

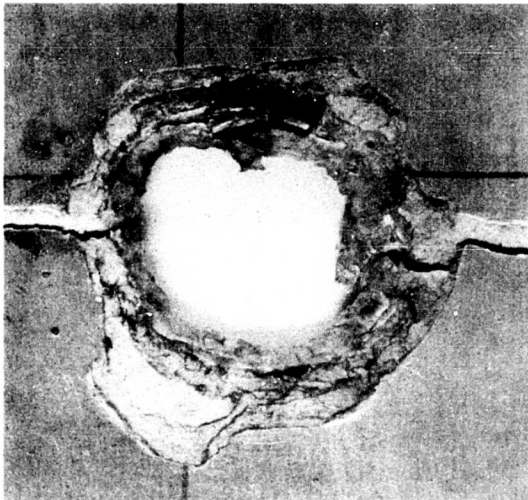
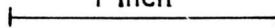


(b) Exit Side

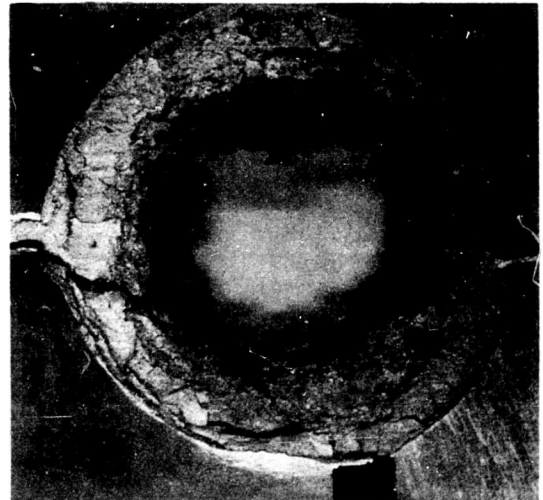
Static Stress 40,000 psi

SCALE

1 Inch



(c) Entrance Side



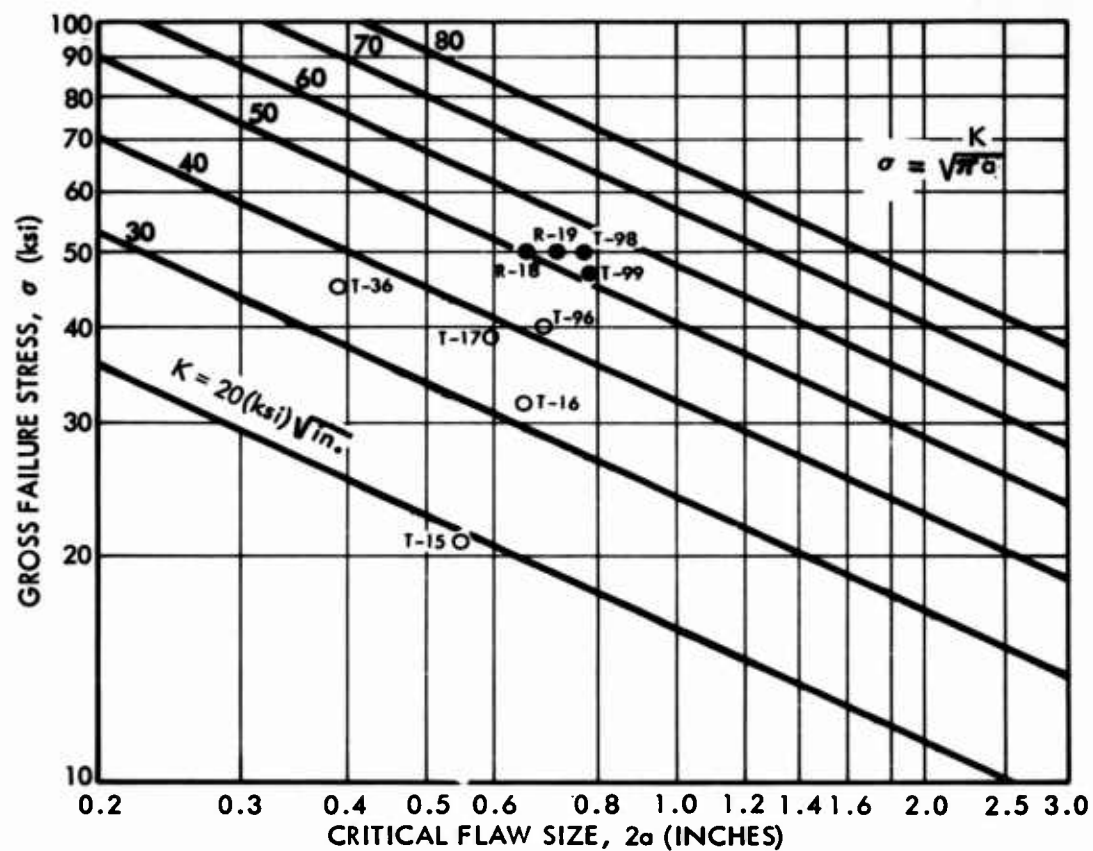
(d) Exit Side

Static Stress 45,700 psi

**Figure 6 FRACTURE MECHANICS TESTS —  
0.400-INCH 7075-T6 SPECIMENS  
1/4-Inch Lexan Cylinder Projectiles**

**CONFIDENTIAL**

**CONFIDENTIAL**



Fracture Occurred    No Fracture



5-Inch Wide Specimen

**Figure 7 FRACTURE STRENGTH OF 0.400-INCH 7075-T6 SPECIMENS**

**CONFIDENTIAL**

## CONFIDENTIAL

provided that the holes produced by hypervelocity impact are sufficient in size; and (2) the fracture toughness for the specimen fractured under hypervelocity impact seems to have a higher value than that produced by laboratory static tests.

### 0.900-Inch 7075-T6 Specimens

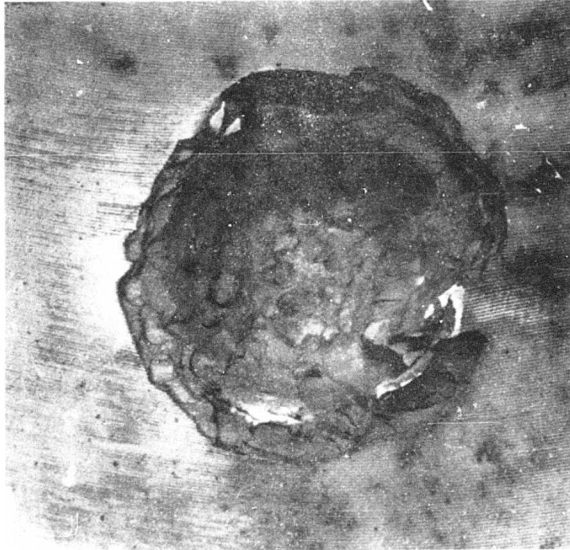
This series of tests was designed to extend the applicability of fracture mechanics concepts to additional hypervelocity impact phenomena. An attempt was made to produce plane-strain fracture failures due to surface flaws, where the crater formed by the projectile impact is considered as the flaw. Projectiles used were 1/8-inch diameter aluminum and 1/4-inch diameter aluminum cylinders.

No fractures were induced by the impacts. However, one specimen that had been impacted by a 1/4-inch aluminum cylinder fractured when a very slight increase of load was applied during the jig unloading procedure. The net stress for this specimen was calculated as 55,600 psi. This indicates a fracture toughness value of at least 45 ksi  $\sqrt{\text{in.}}$ . Even with an additional stress due to jig unloading, the total stress failure was still far below the ultimate strength of the material. The fracture was a plane-strain failure. A photograph of this specimen is shown in Figure 8b. A standard static test of this same material using a notched round specimen resulted in a fracture toughness value of 31 ksi  $\sqrt{\text{in.}}$ . This series of tests has demonstrated that craters produced by hypervelocity impact may behave like surface flaws in producing catastrophic plane-strain fractures at stresses below the material yield strength. However, the fracture toughness value due to hypervelocity impact appears to be higher than that obtained from the static tests. This is consistent with the results of the previous test series.

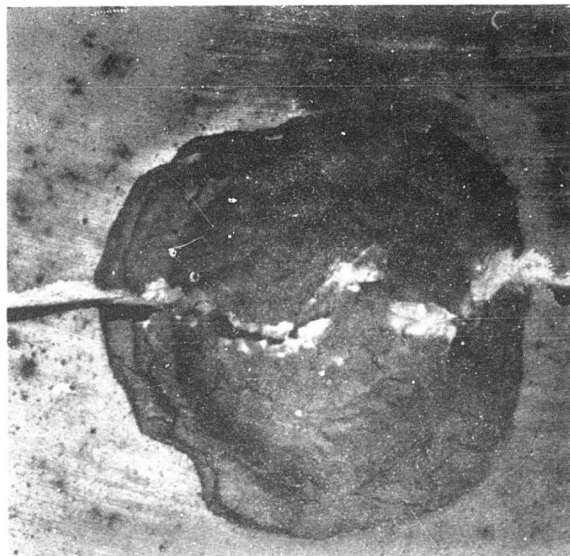
### Ladish D6AC Specimens

This series of tests was designed to investigate the applicability of fracture mechanics to another brittle material having a metallurgical structure different from that of 7075-T6 aluminum. Impact tests have been performed on 0.250-inch thick specimens with 1/4-inch aluminum spheres as projectiles. These tests were planned to obtain the through-the-thickness plane-strain failure mode. No fractures were produced by the tests. The gross static stress applied to the specimens has been as high as 144,000 psi, corresponding to a net-area stress of 197,000 psi. Figure 9 shows the typical results. A minimum fracture toughness value of at least 139 ksi  $\sqrt{\text{in.}}$  was indicated by the impact tests. A standard static test of this particular heat-treat material produced a fracture toughness of 61.5 ksi  $\sqrt{\text{in.}}$ . The static test also gave the yield strength of the material as 257,000 psi and an ultimate strength of 275,000 psi. This series of tests did not produce fractures; the results seem to indicate that a higher plane-strain fracture toughness value is obtained for the specimens under hypervelocity impact.

**CONFIDENTIAL**



(a) Static Stress 30,300 psi



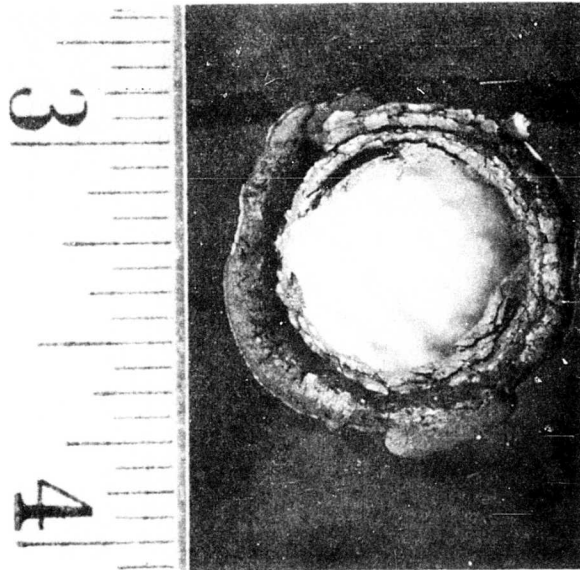
SCALE:  
1/2 Inch

(b) Static Stress 42,500 psi

**Figure 8 FRACTURE MECHANICS TESTS -  
0.900-INCH 7075-T6 SPECIMENS  
1/4-Inch Aluminum Projectiles**

**CONFIDENTIAL**

**CONFIDENTIAL**



(a) Entrance Side



(b) Exit Side

SCALE:  
1/2 Inch

**Figure 9 FRACTURE MECHANICS TESTS -  
0.250-INCH LADISH D6AC SPECIMENS**

1/4-Inch Aluminum Sphere Projectile  
Static Stress 143,500 psi

17

**CONFIDENTIAL**

## CONFIDENTIAL

### V. PHASE II TEST RESULTS

Typical spacecraft pressure vessel configurations consist of a stressed shell covered with a layer of insulation for thermal control and an outer covering, usually metallic, to maintain structural integrity during handling, launch, and orbital operations. As reported in Reference 1, the majority of the existing theoretical or experimental penetration studies have been of thick, or semi-infinite, targets. The experiments involving thin-sheet and shielded targets have been limited and little more than exploratory in scope. An important parameter completely missing in the majority of these studies, one that will be present in any pressure vessel regardless of the contents, is stress. It is the purpose of the Phase II testing to investigate the effect of hypervelocity impact on stressed thin-sheet arrays simulating practical spacecraft configurations.

The penetration phenomena associated with hypervelocity impact on shielded and unshielded structures are manifold and complex. Experimental studies can lead to an impossibly large test program, even if only a few of the most practical configurations are considered. The Phase II test program has been designed to obtain the necessary data with a reasonable number of tests. The methodology adopted has been to investigate one variable at a time. Correlation of the results of each series of tests has provided the insight necessary to define subsequent testing.

One of the primary factors investigated by the Phase II tests is the effect of static stress on hypervelocity impact damage. The material for all of these tests was 2014-T6 aluminum, a typical weldable alloy. Tests have been designed to evaluate the interaction between static stress and hypervelocity impact phenomena. A second factor investigated is the effect of varying shield thickness. Other factors examined have been the additional effects of insulation-type fillers between the shield and the stressed sheets, and of a thick organic slab placed against the back of the stressed specimen. The latter is intended to simulate the effect of propellants on tank structural response subsequent to a hypervelocity impact.

Based upon fracture mechanics criteria, it was not anticipated that catastrophic fracture of the stressed specimens would result when they were impacted directly by any single projectile up to the 1/4-inch maximum diameter used in this program. However, some specimens have fractured, indicating a greater susceptibility to impact damage than originally believed. The Phase II test data are summarized in Table 2. The results of the several series of Phase II tests are discussed below.

#### Single-Sheet Specimens

The 2014-T6 aluminum sheets used for this series of tests ranged in thickness from 0.090-inch to 0.750-inch. They were preloaded to static stresses of 40,

CONFIDENTIAL

Test No.	STRESSED SPECIMEN					SHIELD			PROJECTILE				FIG NO.	NOTES		
	Width & Thick. (inches)	Matl	Stress (psi)	Crater Dia (inches)	Damage Dia (inches)	Failure Mode	Thick. (inches)	Matl	Spacing (inches)	Filler Hole Dia (inches)	Type	Dia (inches)			Matl Mass (grams)	Vel (fps)
T-91	5 .090	2014-T6	23,900	P .34		NF					SP	1/8	Al	.05	16,556	11
R-83	5 .090	2014-T6	36,200	P		NF					SP	1/8	Al	.05	16,579	5
T-86	5 .090	2014-T6	36,800	P .35		NF					SP	1/8	Al	.05	17,341	11,13
T-77	5 .090	2014-T6	47,000	P .36		NF					SP	1/8	Al	.05	16,714	11,33
R-74	5 .090	2014-T6	48,000	C .15		NF					SP	1/8	Al	.05		6
R-72	5 .090	2014-T6	48,000	P .31		NF					SP	1/8	Al	.05	12,405	7
T-150	5 .090	2014-T6	48,300	P .53		NF					SP	1/4	Al	.37	15,252	33
T-115	5 .160	2014-T6	24,300	P .32		NF					SP	1/8	Al	.05	15,300	13
T-44	5 .160	2014-T6	35,400	P .40		NF					SP	1/8	Al	.05	18,190	8
T-113	5 .160	2014-T6	36,400	P .35		NF					SP	1/8	Al	.05	15,600	13,15
T-71	5 .160	2014-T6	45,800	P .36		NF					SP	1/8	Al	.05	15,322	7
R-42	5 .160	2014-T6	47,000	P .27		NF					SP	1/8	Al	.05	11,107	
R-179	5 .250	2014-T6	0	P .31		NF					SP	1/8	Al	.05	15,488	
T-112	5 .250	2014-T6	36,700	P .32		NF					SP	1/8	Al	.05	15,400	13
T-111	5 .250	2014-T6	47,500	P .31		NF					SP	1/8	Al	.05	15,400	13
T-46	5 .375	2014-T6	24,000	P .40		NF					SP	1/8	Al	.05	17,550	13
T-51	5 .375	2014-T6	35,700	C .40		NF					SP	1/8	Al	.05	15,182	13,14
R-48	5 .375	2014-T6	35,900	C .35		NF					SP	1/8	Al	.05	16,440	9
R-47	5 .375	2014-T6	37,000	C .40		NF					SP	1/8	Al	.05		3
T-235	5 .388	2014-T6	35,700	P .64		NF					SP	1/4	Al	.37	15,038	15
T-183	5 .750	2014-T6	17,800	C .72		NF					SP	1/4	Al	.37	15,662	14
T-117	5 .090	2014-T6	48,000	P .15	1.10	FR	.020	7075-T6	2	.19	SP	1/8	Al	.05	15,000	17,35
T-316	8 .090	2014-T6	46,800	P 1.03	1.60	NF	.020	7075-T6	2	.31	SP	1/4	Al	.38	18,360	
R-80	5 .090	2014-T6	48,200	C .05	2.00	NF	.040	2014-T6	2	.26	SP	1/8	Al	.05	16,155	21
T-95	5 .090	2014-T6	47,900	C .12	1.30	F	.040	2014-T6	2	.28	SP	1/8	Al	.05	15,707	21
R-180	5 .090	2014-T6	48,400	C .07	1.50	NF	.040	2014-T6	2	.23	SP	1/8	Al	.05	15,472	17,21,35

**TABLE 2 - PHASE II TESTS**

Sheet 1 of 2

P = Complete Penetration  
C = Crater, No Penetration  
F = Specimen Fractured During Impact Event  
NF = Specimen Did Not Fracture  
FR = Specimen Fractured While Being Removed From the Jig  
SP = Spherical Projectile  
? = No Velocity Measurement

5 Projectile Ricocheted From Jig  
6 Projectile Broke Up  
7 Velocity Slow  
8 Velocity Fast  
9 Sighting Target Left on Specimen  
10 Crater 0.42-inch-Deep, Specimen Spalled  
13 Sighting Target

TABLE 2 - PHASE II TESTS  
Sheet 1 of 2

P = Complete Penetration  
C = Crater, No Penetration  
F = Specimen Fractured During Impact Event  
NF = Specimen Did Not Fracture  
FR = Specimen Fractured While Being Removed From the Jig  
SP = Spherical Projectile  
3 = No Velocity Measurement  
5 = Projectile Ricocheted From Jig  
6 = Projectile Broke Up  
7 = Velocity Slow  
8 = Velocity Fast  
9 = Sighting Target Left on Specimen  
10 = Crater 0.42-inch-Deep, Specimen Spalled  
13 = Sabot Impacted Target

CONFIDENTIAL



CONFIDENTIAL

Test No.	STRESSED SPECIMEN						SHIELD			PROJECTILE					FIG NO.	NOTES			
	Width & Thick. (inches)	Matl	Stress (psi)	Crater Dia (inches)	Damage Dia (inches)	Failure Mode	Thick. (inches)	Matl	Spacing (inches)	Filler	Hole Dia (inches)	Type	Dia (inches)	Matl			Mass (grams)	Vel (fps)	
T-151	5 .090	2014-T6	48,000	P .80	1.35	F	.040	2014-T6	2			.39	SP	1/4	Al	.37	15,000	16	
T-89	5 .090	2014-T6	36,200	C .10	1.50	NF	.090	2014-T6	2			.35	SP	1/8	Al	.05	16,322	17	
T-78	5 .090	2014-T6	48,200	C .10	2.00	NF	.090	2014-T6	2			.35	SP	1/8	Al	.05	15,877	11	13
T-152	5 .090	2014-T6	48,600	P .35	2.25	F	.090	2014-T6	2			.54	SP	1/4	Al	.37	14,829	16,22	
R-79	5 .090	2014-T6	48,000	C .08	1.50	NF	.160	2014-T6	2			.27	SP	1/8	Al	.05		2	
T-81	5 .090	2014-T6	47,300	C .11	1.50	NF	.160	2014-T6	2			.34	SP	1/8	Al	.05	16,177	17	13
T-158	5 .090	2014-T6	0	P .70	2.25	FC	.160	2014-T6	2			.60	SP	1/4	Al	.37	15,134	19,35	11
T-157	5 .090	2014-T6	12,300	P .80	2.25	F	.160	2014-T6	2			.62	SP	1/4	Al	.37	14,985	19	
T-155	5 .090	2014-T6	23,500	P .75	2.25	F	.160	2014-T6	2			.62	SP	1/4	Al	.37	15,345	19	
T-154	5 .090	2014-T6	36,500	P 1.10	2.25	F	.160	2014-T6	2			.59	SP	1/4	Al	.37	14,925	19	
T-153	5 .090	2014-T6	48,100	P .60	2.25	F	.160	2014-T6	2			.60	SP	1/4	Al	.37	14,844	16,19	
T-214	5 .090	2014-T6	48,500	P .14	1.80	F	.250	2014-T6	2			.71	SP	1/4	Al	.37	15,663	16,23	
T-122	5 .090	2014-T6	48,000	C .16		NF	.020	7075-T6	2	Q-Felt		.18	SP	1/8	Al	.05	15,000	24	
T-131	5 .090	2014-T6	48,000	C .10		NF	.040	2014-T6	2	Q-Felt		.25	SP	1/8	Al	.05	15,408		
T-182	5 .090	2014-T6	48,400	C .16		NF	.160	2014-T6	2	C-Felt		.63	SP	1/4	Al	.37	15,373	24	
T-120	5 .090	2014-T6	47,300	P .31		NF							SP	1/8	Al	.05	15,800	16	
T-212	5 .090	2014-T6	38,500	P .32		NF							SP	1/8	Al	.05	15,516	25,27	16
T-324	5 .090	2014-T6	48,100	P .58		F							SP	1/4	Al	.38	16,238	26,27	12 16
T-118	5 .020	2014-T6	46,900	P .28		NF							SP	1/8	Al	.05	15,300		16

TABLE 2 - PHASE II TESTS  
Sheet 2 of 2

P = Complete Penetration  
C = Crater, No Penetration  
F = Specimen Fractured During Impact Event  
NF = Specimen Did Not Fracture  
FC = Specimen Suffered a Major, Critical Crack Due to Impact  
SP = Spherical Projectile  
2 Crater Too Far Off Center  
11 Total Crack Length 4 Inches  
12 Specimen Shattered by Shock Wave in Paraffin  
13 Sabot Impacted Target  
16 Paraffin Block Attached to Back of Stressed Specimen

## CONFIDENTIAL

60, or 80 percent of the material nominal yield strength. The projectiles used were 1/8- and 1/4-inch diameter aluminum spheres of 0.05- and 0.38-gram masses respectively; impact velocities were approximately 16,000 feet per second. The test results reveal that there is no noticeable change in crater configuration due to the application of static stresses. As shown in Figure 10, holes of practically the same size are produced in targets of equal thickness but subjected to various stresses. One typical set of craters is shown in Figure 11. The photographs show the holes formed in 0.090-inch sheets tested at four different stress levels.

Figure 12 shows that the effect of stress and of target thickness on hole size can be depicted by a single curve. Photographs of a typical series from this curve are shown in Figure 13. Sheets loaded to 60-percent yield stress and of thicknesses between 0.090 and 0.375 inch were impacted by 1/8-inch aluminum spheres. The damage produced on stressed and unstressed targets is indistinguishable. Further reinforcement of this thesis is obtained from the craters and holes shown in Figures 14 and 15. The first of these figures shows a comparison between the crater in a 0.375-inch stressed sheet due to a 1/8-inch sphere, and that in a 0.75-inch stressed sheet due to a 1/4-inch sphere; the sheet-thickness-to-projectile-diameter ratios for both are the same. Figure 15 shows penetration of a 1/4-inch sphere through a 0.375-inch stressed sheet, and of an 1/8-inch sphere through a 0.160-inch stressed sheet. The damage shown in both these figures is the same as would have been produced in unstressed specimens.

These results confirm that it is not physically possible for the material to adjust deformation instantaneously to the application of transient stresses. If transient impact stresses do not persist long enough for the material to respond, only static stress systems need be considered in evaluation of failure modes. For example, a crater or hole will be generated in an aluminum target under hypervelocity impact in less than 50 microseconds. This is less than the effective response time of aluminum, defined as a maximum crack propagation distance; hence, the crater can be treated as a static stress concentration or flaw. The seriousness of the stress-concentration effect depends on the stress level, the microcosmic geometry of the flaw, and on the material behavior.

### Shielded Specimens

The shielded specimen tests have been performed with a constant 2-inch stand-off spacing. The stressed specimen has been an 0.090-inch thick 2014-T6 aluminum sheet. Stress level for all but a few tests was 80 percent of nominal material yield. The projectile was either an 1/8-inch or a 1/4-inch aluminum sphere, launched at approximately 16,000 feet per second. The width of the stressed sheet was 5 inches for all 1/8-inch projectile tests and most of the 1/4-inch projectile tests. Several 8-inch wide specimens have also been tested in order to study specimen edge effects.

CONFIDENTIAL

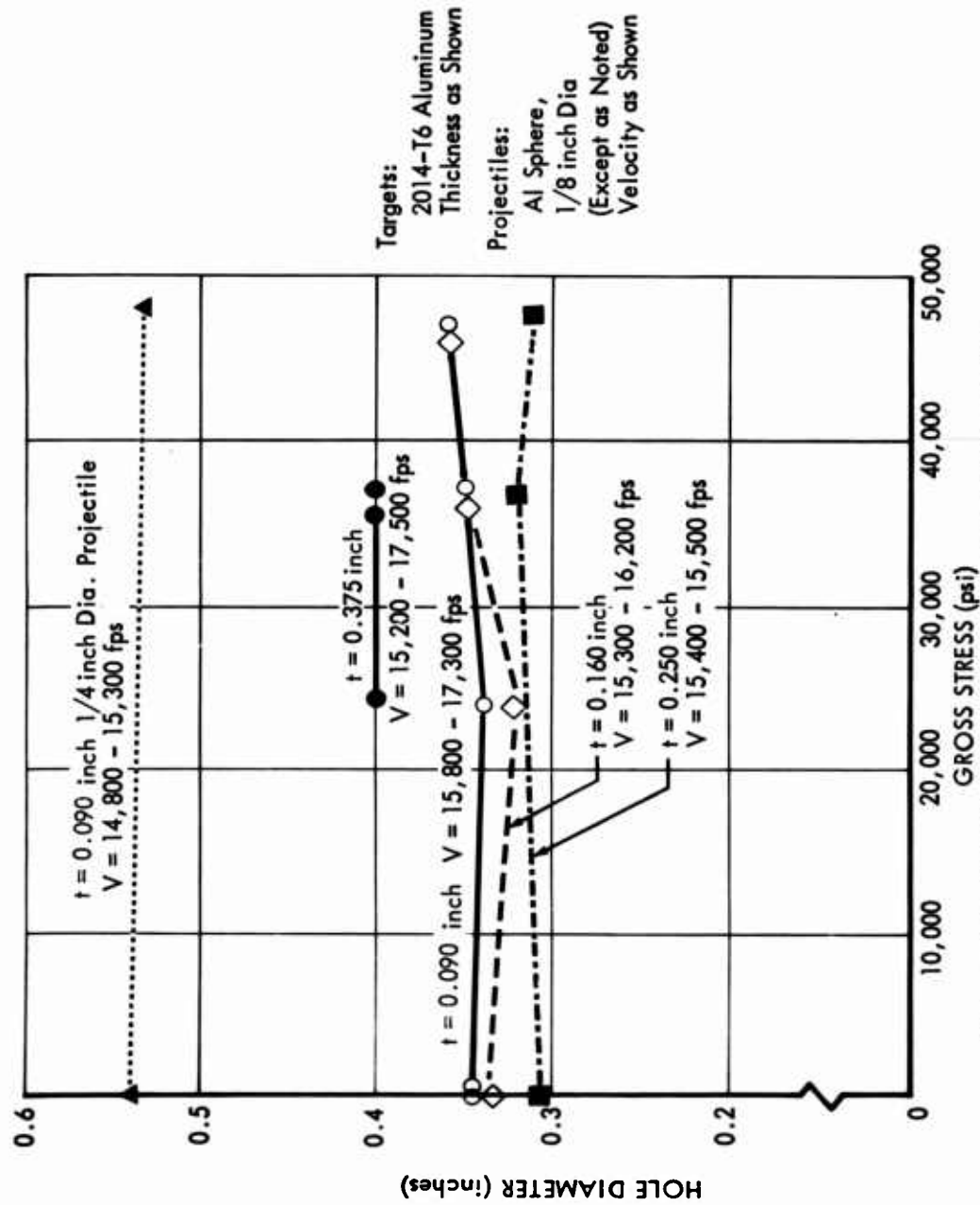
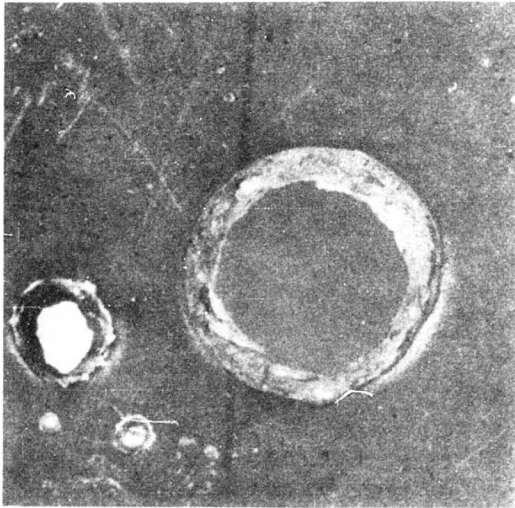
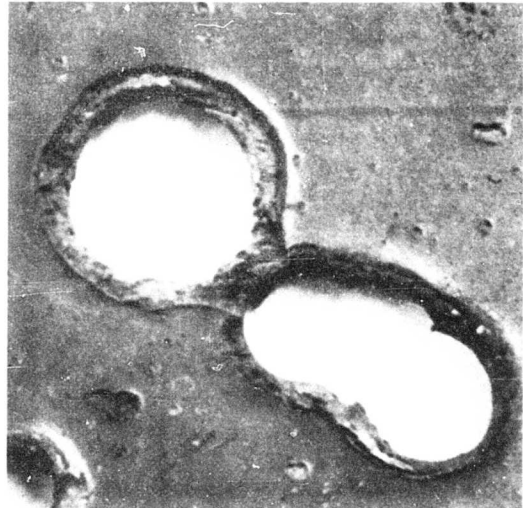


Figure 10 EFFECT OF TARGET STRESS ON HOLE SIZE



(a) Static Stress 0 psi

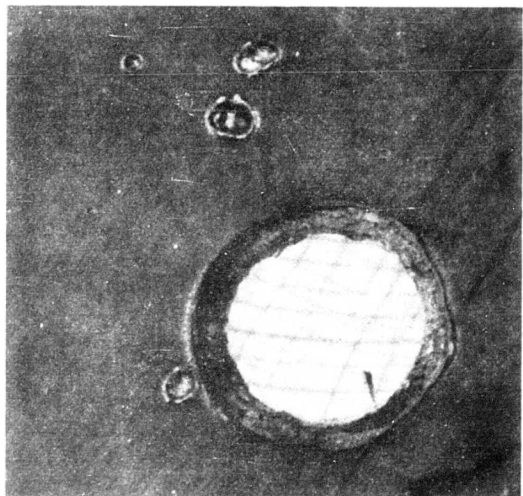


(b) Static Stress 23,900 psi  
(40% Yield)

SCALE:  1/2 Inch



(c) Static Stress 36,800 psi  
(60% Yield)



(d) Static Stress 47,000 psi  
(80% Yield)

**Figure 11 EFFECT OF STATIC STRESS ON UNSHIELDED SPECIMENS**

0.090-Inch 2014-T6 Specimens  
1/8-Inch Aluminum Sphere Projectile

CONFIDENTIAL

Projectile Velocity: 14,500 fps to 16,700 fps  
 Target Stress: Various Stress Level, From No Stress to 90% Yield  
 ○ 1/8" Al Sphere, 0.05 gm, Impacted on 2014-T6 Specimen  
 ⊗ 1/8" Al Sphere, 0.05 gm, Impacted on 7075-T6 Specimen  
 ○ 1/8" Al Sphere, 0.05 gm, Impacted on 2014-T6 Tank  
 ● 1/4" Al Sphere, 0.37 gm, Impacted on 2014-T6 Specimen  
 △ 1/4" Al Cylinder, 0.48-0.49 gm, Impacted on 7075-T6 Specimen  
 □ 1/4" Al Cylinder, 0.54 gm, Impacted on 7075-T6 Specimen  
 ● 1/4" Al Sphere, 0.38 gm, Impacted on 2014-T6 Tank

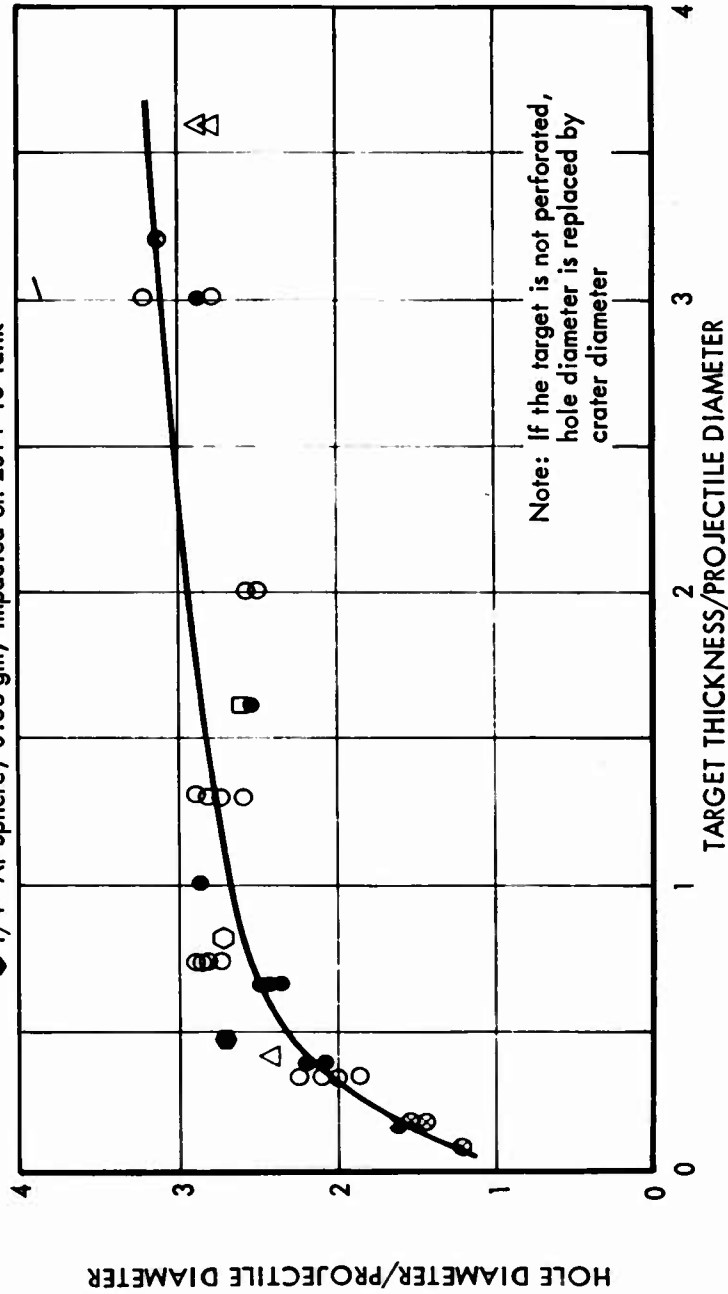


Figure 12 EFFECT OF TARGET THICKNESS ON HOLE SIZE

CONFIDENTIAL

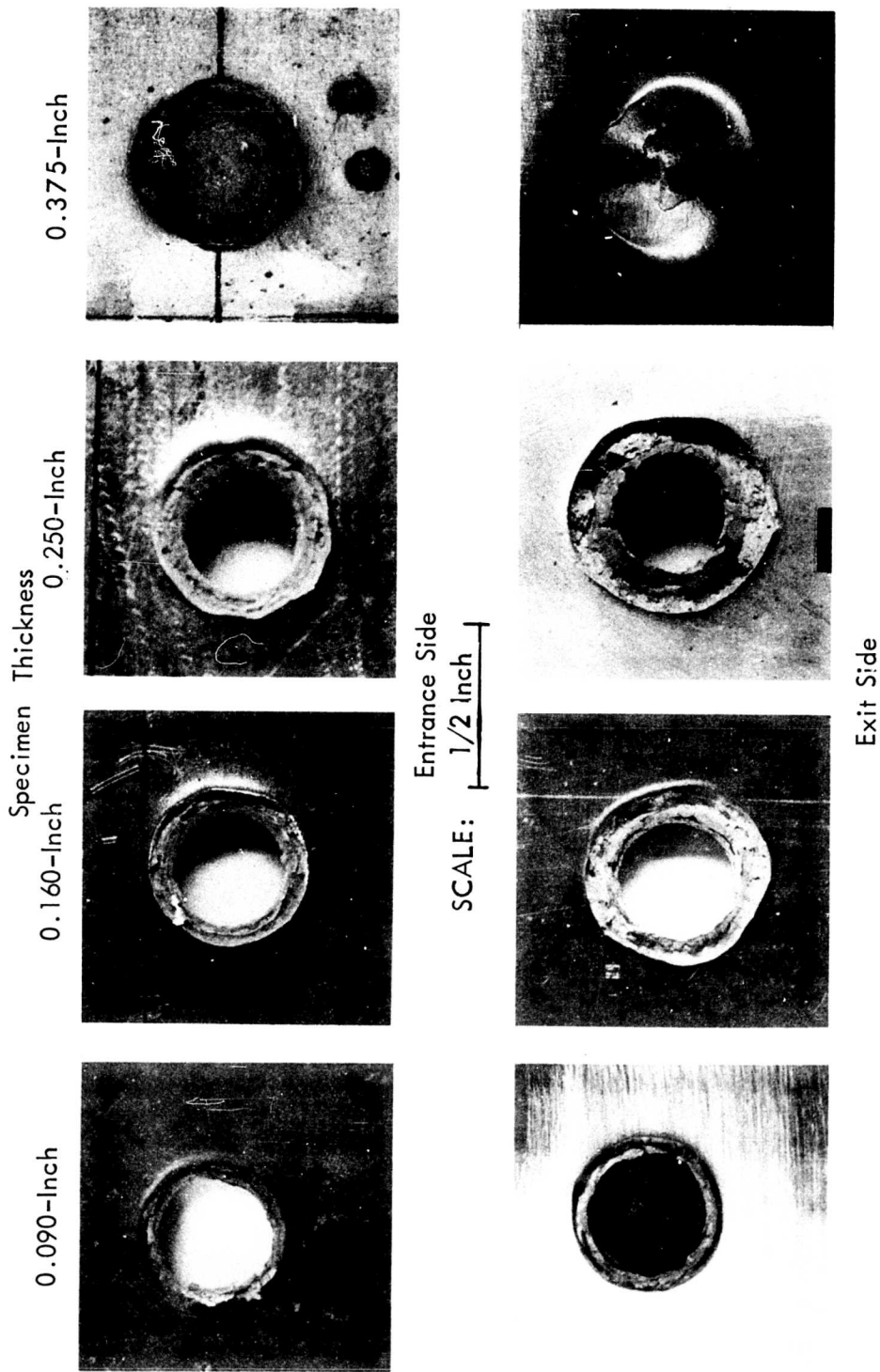


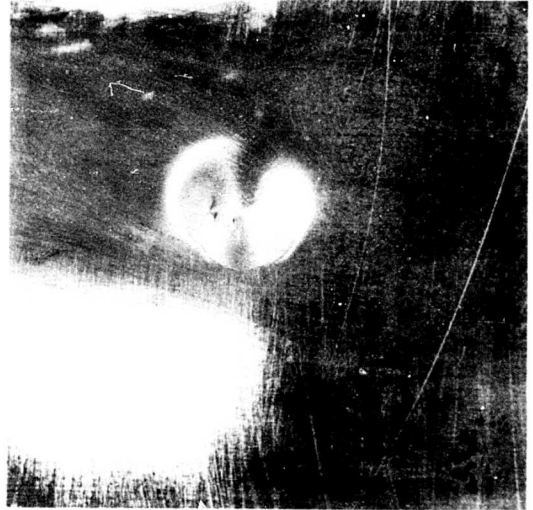
Figure 13 EFFECT OF TARGET THICKNESS ON IMPACT DAMAGE

2014-T6 Specimens

1/8-Inch Aluminum Sphere Projectiles

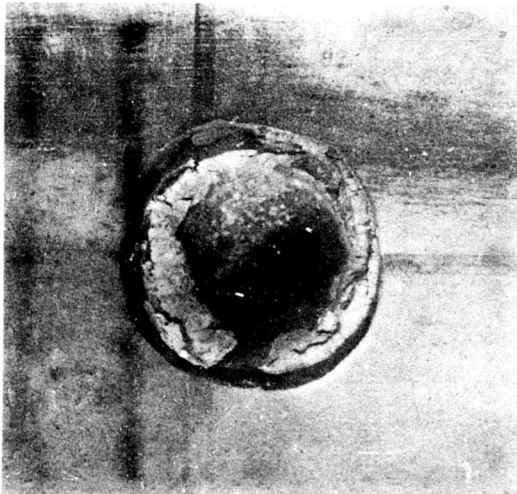
Static Stress 60% Yield

**CONFIDENTIAL**



0.375-Inch 2014-T6 Specimen  
Static Stress 35,700 psi 1/8-Inch Projectile

SCALE:  
1 Inch



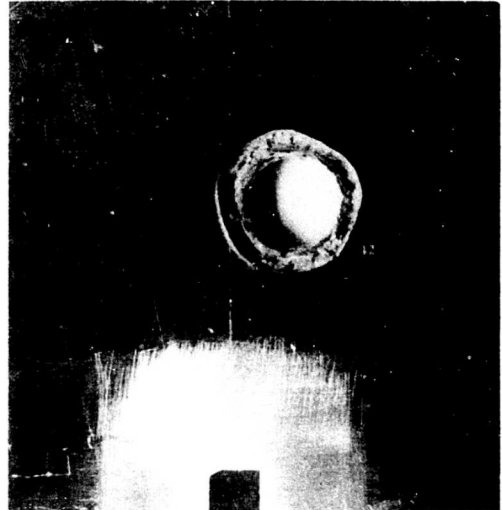
0.750-Inch 2014-T6 Specimen  
Static Stress 17,800 psi 1/4-Inch Projectile


## Figure 14 PROJECTILE AND TARGET SCALING - CRATERS

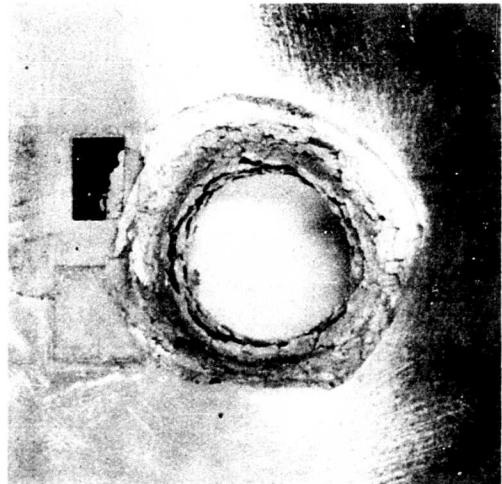
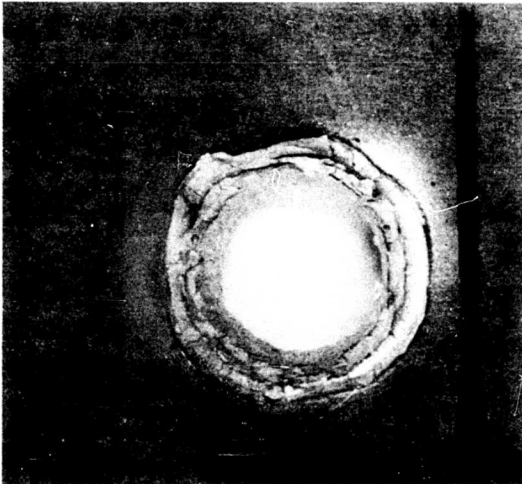
Aluminum Sphere Projectiles  
Sheet-Thickness/Projectile-Diameter Ratio = 3.00

**CONFIDENTIAL**

**CONFIDENTIAL**



0.160-Inch 2014-T6 Specimen  
1/8-Inch Projectile  
Sheet-thickness/Projectile-Diameter Ratio = 1.28  
SCALE: 



0.375-Inch 2014-T6 Specimen  
1/4-Inch Projectile  
Sheet-Thickness/Projectile-Diameter Ratio = 1.50

**Figure 15 PROJECTILE AND TARGET SCALING - PENETRATIONS**

Aluminum Sphere Projectiles  
Static Stress 60% Yield

**CONFIDENTIAL**



## CONFIDENTIAL

Results of the shielded specimen tests may be summarized as follows:

- 1) Under certain conditions, an unshielded specimen can sustain impact damage from a hypervelocity projectile without fracturing, but the addition of a shield breaks up the projectile, spreads the damage over a larger area, and causes the specimen to fracture catastrophically.
- 2) The damage area of the shielded specimen is a function of shield thickness; thicker shields tend to increase the damaged area.
- 3) Increasing the shield thickness generates larger ejecta or spall fragments. Fewer but larger and deeper craters are produced in the shielded target.

These results are valid only within certain thickness limits of the shield, since a sufficiently thick shield will completely stop the projectile.

Figure 16 shows damage to stressed targets by 1/4-inch projectiles after penetrating shields of various thicknesses. In each of the tests shown in Figure 16, there are signs of light ejecta impacts extending over an area 4 to 5 inches in diameter; this damage is considered structurally insignificant when compared to the damage clustered nearer the center of impact. Figure 16a shows a target after a 1/4-inch projectile impacted through a 0.040-inch shield. This produces a 0.80-inch diameter hole in the target while the ejecta damages a 1.30-inch diameter area surrounding the hole. Increasing the shield thickness to 0.090 inch, as shown in Figure 16b, increases the ejecta damage diameter to about 2.25 inches while the central hole diameter decreases. Typical crater diameters in the damaged area are about 0.05 inches.

Increasing the shield thickness to 0.160 inch, as shown in Figure 16c, produced the same damage area but the diameter of the individual craters in the stressed specimen has increased to approximately 0.10 inch. Figure 16d shows a 0.250-inch thick shield test. The damage diameter is 1.80 inches; the fewer but larger craters within this area are 0.12 to 0.15 inch in diameter. If the stressed specimen had not been shielded, the impact damage would have been a single hole about 0.53 inch in diameter and the specimen would not have fractured due to the impact.

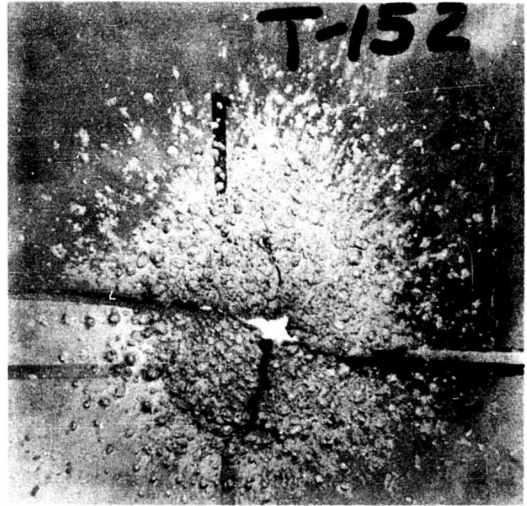
Similar results were obtained for a series using 1/8-inch diameter projectiles, shown in Figure 17. For the 0.020-inch thick shield, Figure 17a, the ejecta damage diameter was 1.1 inches. Other tests for this series produced a damage diameter of 1.5 inches. The diameters of the craters in the damaged area increased with increasing thickness of the shield, e.g., 0.03-, 0.06- and 0.10-inch diameter craters for 0.040-, 0.090-, and 0.160-inch shield thicknesses, respectively. Typical unshielded stressed specimen damage is shown in Figure 11; the holes are all about 0.35 inch in diameter.

The effects of increasing shield thickness can also be shown graphically, as in Figure 18; data on normalized target damage area is plotted against

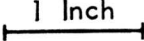
**CONFIDENTIAL**



(a) 0.040-Inch Shield



(b) 0.090-Inch Shield

SCALE:  1 Inch



(c) 0.160-Inch Shield



(d) 0.250-Inch Shield

**Figure 16 EFFECT OF SHIELD THICKNESS - 1/4-INCH PROJECTILE**

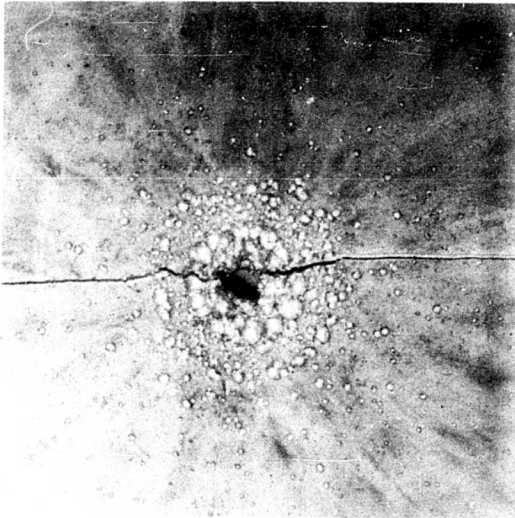
2014-T6 Specimens

Static Stress 80% Yield

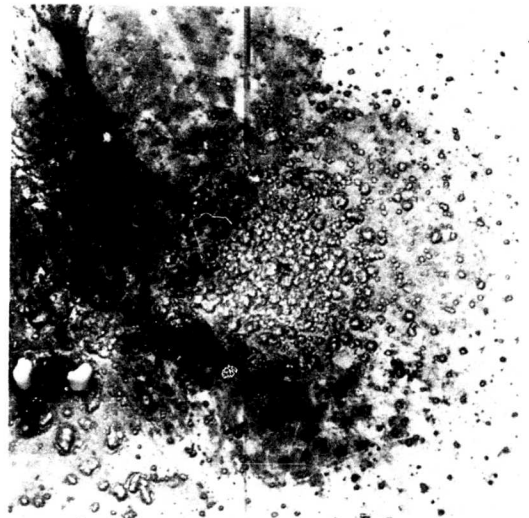
29

**CONFIDENTIAL**

**CONFIDENTIAL**



(a) 0.020-Inch Shield



(b) 0.040-Inch Shield

SCALE: 1 Inch



(c) 0.090-Inch Shield



(d) 0.160-Inch Shield

## Figure 17 EFFECT OF SHIELD THICKNESS - 1/8-INCH PROJECTILE

2014-T6 Specimens  
Static Stress 80% Yield

30

**CONFIDENTIAL**

CONFIDENTIAL

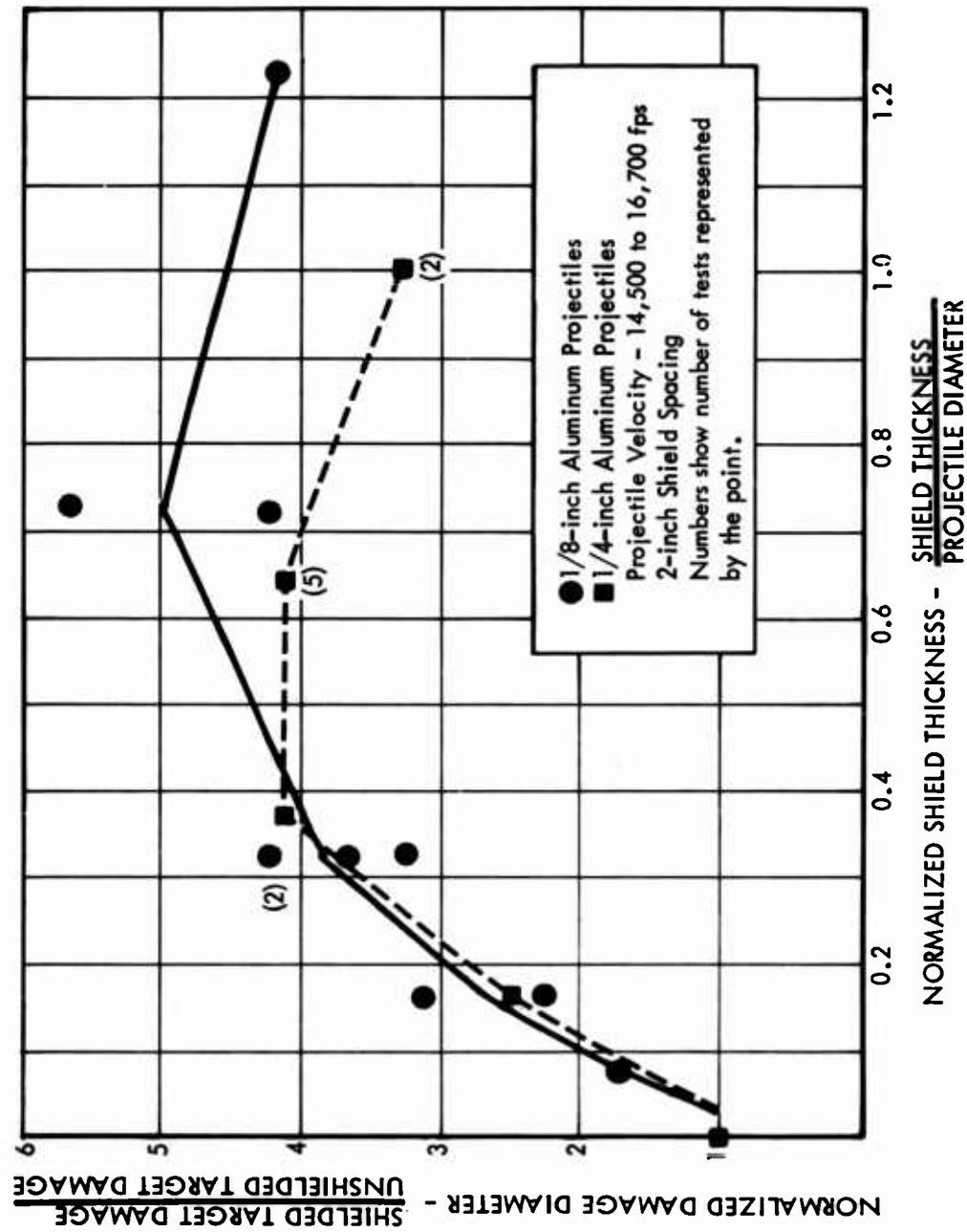


Figure 18 SHIELDED SPECIMEN DAMAGE VS. SHIELD THICKNESS

CONFIDENTIAL

## CONFIDENTIAL

normalized shield thickness. Target damage area is normalized by using the damage area produced by an identical projectile impacting an unshielded target. As shield thicknesses approach zero, the curves converge to unity, i.e., the damage is the same as that formed in an unshielded specimen. As shield thicknesses increase, the damage diameter first increases, then levels off, and eventually falls to zero when the projectile fails to penetrate.

For extremely thin shields, i.e., shield-thickness-to-projectile-diameter ratios of 0.05 or less, there are no indications of projectile break-up. The hole in a shielded specimen is the same as that of an unshielded specimen. Shields having shield-to-projectile ratios of 0.05 to 0.20 break up the penetrating projectile. The fragments remain relatively clustered and produce holes in the second sheet that are up to 70 percent larger than the holes in an unshielded specimen. The edges of these penetrations have the typical appearance common to hypervelocity impact damage. The ejecta damage diameter is usually taken as the largest lip-to-lip dimension of the major penetration. Figure 4b is a typical example of this damage.

Shields with ratios from 0.2 to 1.3, the thickest tested, cause the projectile to shatter and produce many dispersed craters. The ejecta-damage area for this region is highly susceptible to observer judgment, but generally includes most of the larger craters. This is similar to the reduced target damage diameter described in Reference 5. Ejecta from these heavily shielded specimens usually include large chunks of material torn from the target.

The effect of static stress on hypervelocity impact damage to shielded specimens is shown in Figure 19. A series of 0.090-inch 2014-T6 aluminum specimens with 0.160-inch thick shields spaced 2 inches in front were tested using 1/4-inch diameter aluminum spheres. The only variable in this series was the specimen stress level; this ranged from zero to 80 percent of nominal material yield. The impact damage has no distinguishing stress-induced differences. With the exception of the unstressed specimen, all specimens fractured under the projectile impact. The cause of these fractures will be discussed in the next section.

### Fractures

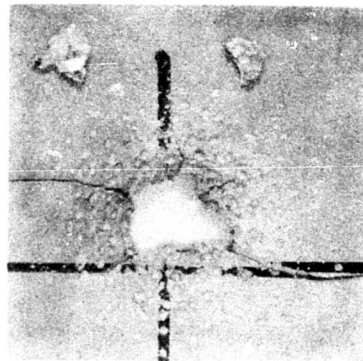
During the original planning of this testing program it was anticipated that fracture of the Phase II specimens due to hypervelocity impact was unlikely. Indeed, none of the unshielded stressed specimens have suffered catastrophic fracture due to the impact of a single projectile. However, the addition of shields, or the impact of several projectiles, e.g., sabot particles, has introduced additional effects, some of which have caused the specimen to fracture.

Figure 20 is a plot of all applicable Phase II data, including both shielded and unshielded tests. The standard fracture mechanics format has been used for this plot. The points marked with an asterisk denote tests that incurred

**CONFIDENTIAL**



(a) 80% Yield Strength

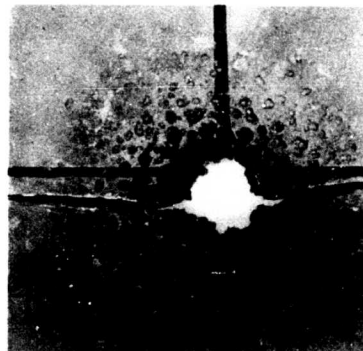


(b) 60% Yield Strength

SCALE:  
1 Inch



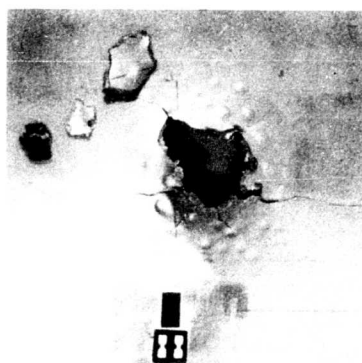
(c) 40% Yield Strength



(d) 20% Yield Strength



(e) No Stress - Front



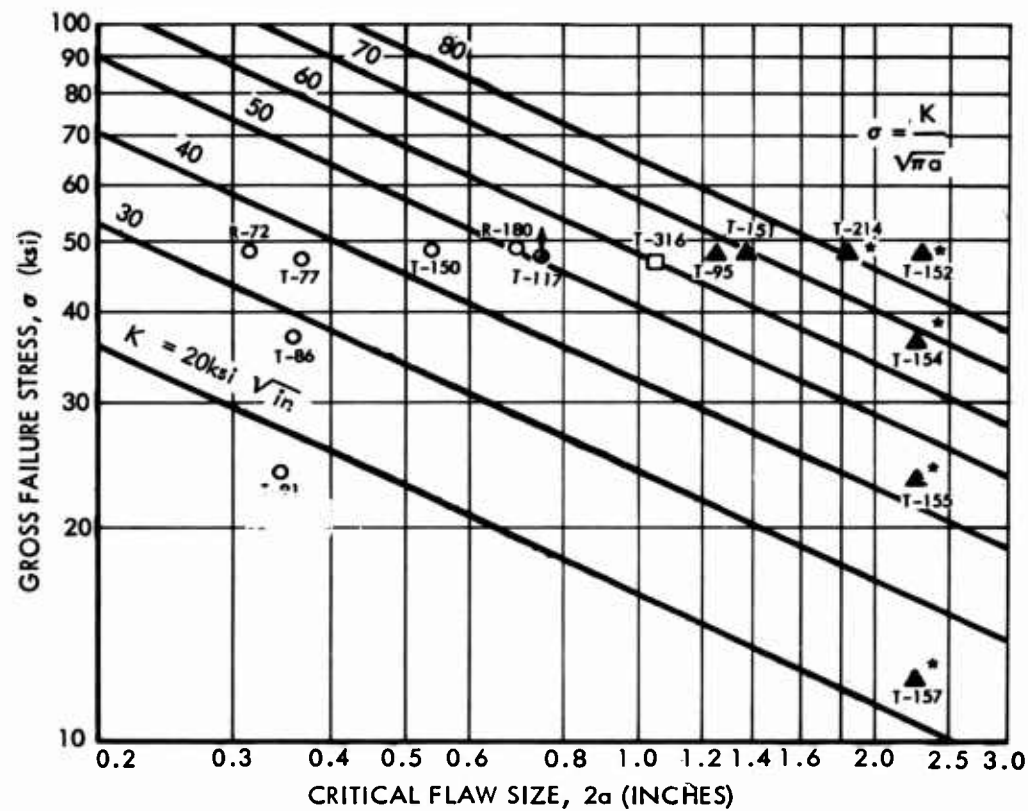
(f) No Stress - Back

**Figure 19 EFFECT OF STATIC STRESS ON SHIELDED SPECIMENS**

0.090-Inch 2014-T6 Specimens 0.160-Inch Shield, 2-Inch Spacing  
1/4-Inch Aluminum Sphere Projectile

**CONFIDENTIAL**

CONFIDENTIAL



Fracture Occurred	No Fracture	
●	○	5-Inch Wide Specimen - No Shield
▲	△	5-Inch Wide Specimen - Various Shields, 2-Inch Spacing
■	□	8-Inch Wide Specimen - Various Shields, 2-Inch Spacing
●		Fracture Occurred During Removal From Jig
*		Specimen Deformed by Impact

Figure 20 FRACTURE STRENGTH OF 0.090-INCH 2014-T6 SPECIMENS

CONFIDENTIAL



## CONFIDENTIAL

large deformations due to the impact; this is a special case to be discussed later. The data without asterisks can be explained using fracture mechanics concepts. Considering all applicable Phase II tests shown in Figure 20, a static fracture toughness value of between 60 and 70  $\text{ksi}\sqrt{\text{in.}}$  is indicated by the data. An examination of the available static fracture toughness data has revealed that the room temperature values are about the same for both 2014-T6 and 7075-T6 aluminum. From this it appears that the impact fracture toughness values indicated by the Phase II tests are not unreasonable.

A series of tests, where specimens with 0.040-inch shields were impacted with 1/8-inch diameter spheres, provided unintentional support for the applicability of the fracture mechanics concept. Each of the three test specimens shown in Figure 21 suffered a sabot impact in addition to the projectile. Except for the unknown size of the sabot fragment, all three tests were nearly identical, but the response after impact was different. Two targets withstood the test and one fractured. The holes in the shields due to the sabot fragment were about the same size for each test, but the fragment behavior after penetration was different. In the first test, Figure 21a, the fragment appeared to be completely broken up and produced a series of craters randomly distributed over a 1.5-inch diameter area. The fragment of the second test, Figure 21b, seemed to remain in larger pieces and produced five penetrations of the stressed sheet. A surface crack on the back side of the specimen connected three of these penetrations forming a crack 0.69 inch long, oriented about 75 degrees from the stress axis. Projected crack length normal to the axis of the stress was 0.62 inch. The fragment in the last test, Figure 21c, not only remained in larger pieces, but it also produced a line of three or four penetrations having a total length of 1.25 inches. There was also considerable damage to the target material between the penetrations. This formed a crack oriented normal to the specimen stress axis. While fracture due to loss of cross-sectional area and associated stress concentrations cannot be excluded, it would take a fracture toughness value of about 67  $\text{ksi}\sqrt{\text{in.}}$  to resist a fracture for these test conditions.

The asterisked data of Figure 20 were fractures that occurred when 1/4-inch spheres impacted specimens with shields 0.090 inch thick or thicker. Face and edge views of a typical fracture are shown in Figure 22. The edge view of the specimen shows the gross deformation normal to the plane of stress produced by the impact. The large deflections induced by the impact are sufficient to produce secondary stress effects that become critical. This is supported by the test shown in Figures 19e and 19f. The unstressed specimen did not completely fracture, but the crack formed by the impact extended over 4 inches of the 5-inch wide specimen.

The specimens used for the above tests were 5 inches wide. Because of possible edge effects, 8-inch specimens were manufactured and tested using a 0.250-inch shield. As shown in Figure 23, the 8-inch specimen suffered the same gross deformation and cracking as a similarly tested 5-inch specimen.



**CONFIDENTIAL**



(a) Test R-80 - No Penetration



(b) Test R-180 - Penetrated and Cracked  
(Crack extends through  
three largest holes)



(c) Test T-95 - Fractured Due to Impact

SCALE:  
1 Inch

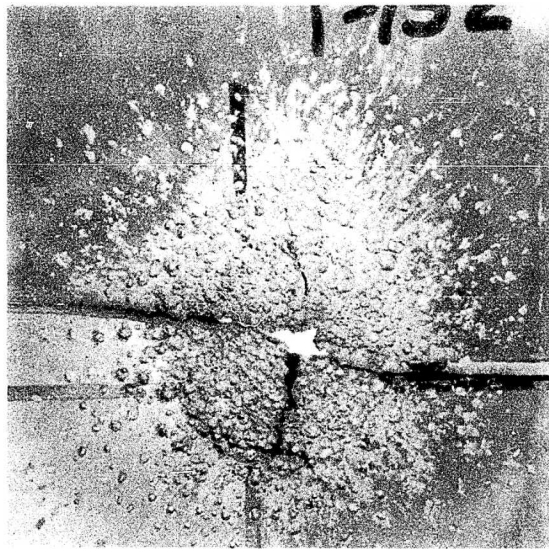
**Figure 21 DAMAGE DUE TO IMPACT  
OF 1/8-INCH PROJECTILE PLUS SABOT**

0.090-Inch 2014-T6 Specimen 0.040-Inch Shield, 2-Inch Spacing

Static Stress 80% Yield

**CONFIDENTIAL**

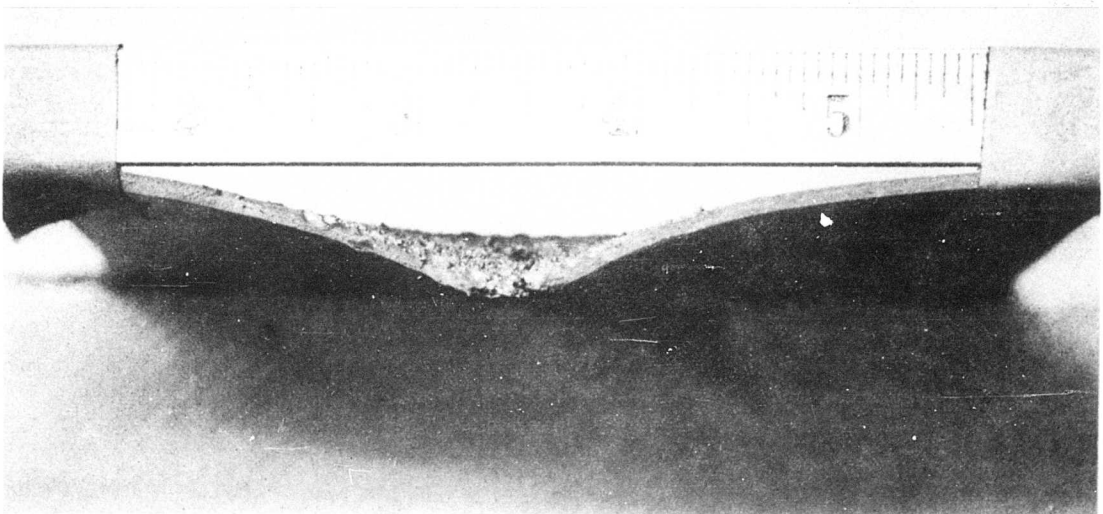
**CONFIDENTIAL**



SCALE:  
1 Inch

(a) Damage to Stressed Sheet

Projectile  
Flight  
Direction



(b) Edge View of Fracture

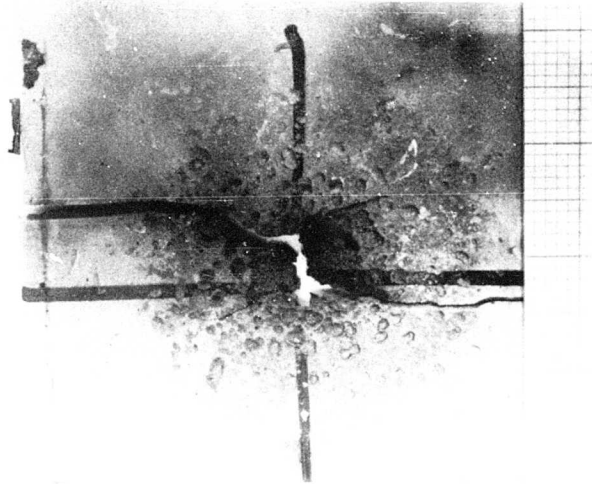
### Figure 22 LARGE DEFLECTION IMPACT DAMAGE

0.090-Inch Shield, 2-Inch Spacing    0.090-Inch 2014-T6 Specimen

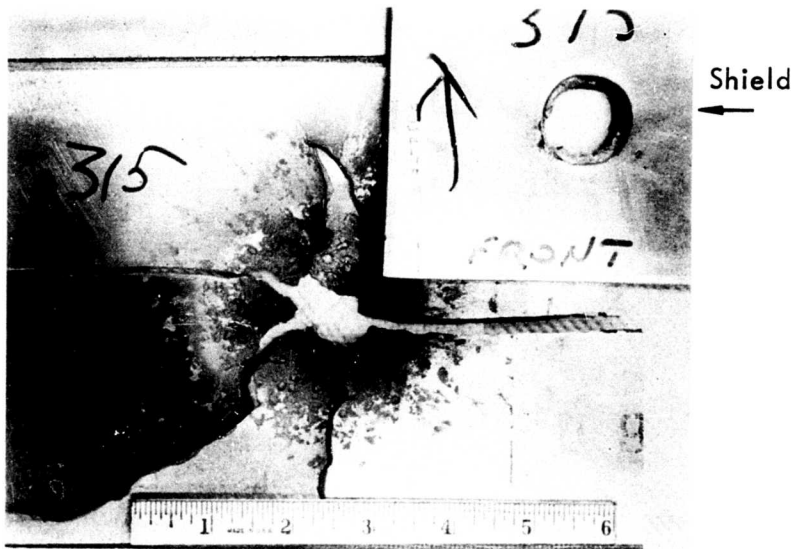
Static Stress 80% Yield

**CONFIDENTIAL**

**CONFIDENTIAL**



(a) 5-Inch-Wide, 0.090-Inch Thick, 2014-T6 Specimen  
Static Stress 48,500 psi



(b) 8-Inch-Wide, 0.100-Inch-Thick, 7075-T6 Specimen  
Static Stress 33,800 psi

**Figure 23 EFFECT OF SPECIMEN WIDTH  
ON LARGE DEFLECTION IMPACT DAMAGE**  
0.250-Inch Shield, 2-Inch Spacing

**CONFIDENTIAL**

## CONFIDENTIAL

It is clear that the specimen geometry has not significantly biased test results.

### Insulation Fillers

Typical spacecraft structure is usually multilayered with at least one layer of low-density, insulation-type filler. A series of tests has been performed to investigate the effectiveness of fillers in defeating hypervelocity projectiles. The standard Phase II shielded specimens and test conditions were used, i.e., 5-inch wide 0.090-inch thick 2014-T6 stressed specimens, static stress 80 percent nominal yield, and various shields at 2-inch spacing. The 2-inch space between the two sheets was filled with four 1/2-inch layers of Q-Felt, a quartz fiber insulation, manufactured by Johns-Manville.

Figure 24 shows results typical of this series; Figure 24a is a photograph of a 0.020-inch shield and the 0.18-inch diameter hole due to a 1/8-inch diameter projectile; the filler is shown in Figure 24b. The damage to the stressed specimen, a crater 0.08 inch deep that did not penetrate the specimen, is shown by Figure 24c. This test can be compared to the specimen shown in Figure 17a, an identical test except for the filler.

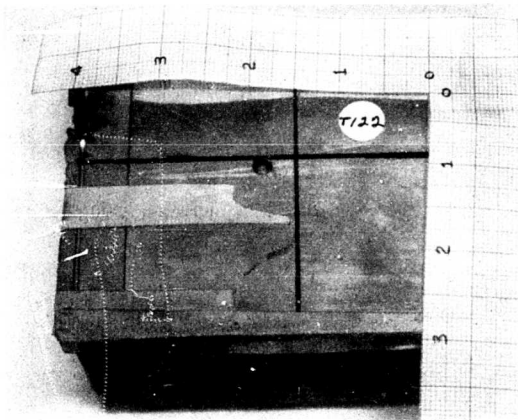
In another test of this series, a 0.160-inch shield and a 1/4-inch diameter spherical projectile were used. This is the same configuration that produced the catastrophic failures and gross deformations shown in Figures 19 and 22. The damage to the stressed specimen used in the test with filler, shown in Figure 24d, was limited to craters that did not penetrate the specimen. The filler successfully defeated the particle, although about 25 cubic inches of the insulation was pulverized and completely destroyed by the impact.

### Backing Media

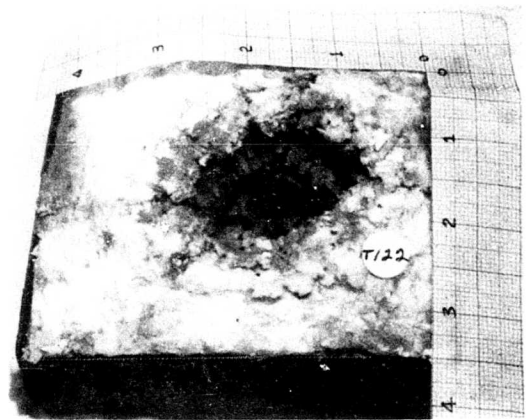
The tests reported above have been designed as screening tests to determine the failure modes of pressure vessels. These tests have been limited to the simulation of gas-filled pressure vessels. The effects of a liquid or solid media contained in a pressure vessel are expected to introduce new phenomena that may overshadow the hypervelocity penetration effects, i.e., the shock pressure induced in continuous media may be sufficient to cause the structure to fracture. A propellant tank, filled with either solid or liquid fuels, is a typical example. Simulation of a solid propellant or an incompressible fluid-filled vessel using uniaxially loaded specimens can be accomplished by placing an appropriate block of material against the back of the stressed sheet. Tests performed at Lewis Research Center, NASA, suggest that paraffin produces the same general effect as water when impacted by a hypervelocity projectile. To study this relation, a series of tests using paraffin blocks on the back of the specimen have been performed. Other backing material such as polyurethane blocks will be used in future tests.

For the first tests, 1/8-inch diameter aluminum spheres were fired into 0.090- and 0.250-inch thick stressed specimens. In each test, the size of the

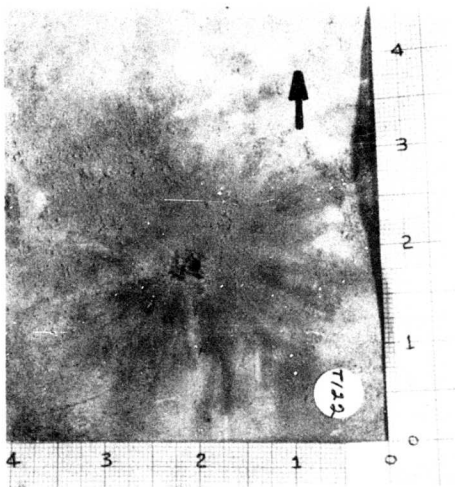
**CONFIDENTIAL**



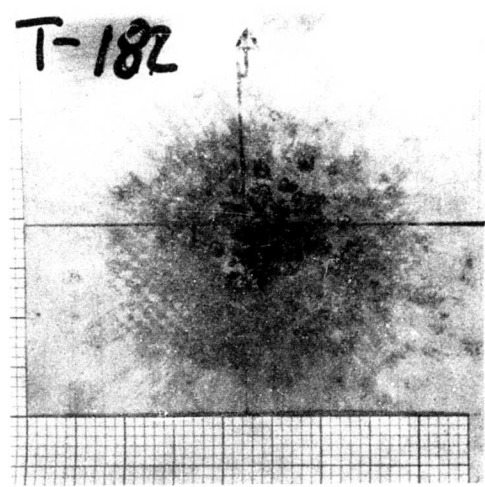
(a) 0.020-inch Shield  
1/8-inch Projectile



(b) Exit Side of 2-inch Q-Felt Filler  
1/8-inch Projectile



(c) 0.090-inch Stressed Specimen  
0.020-inch Shield, 1/8-inch Projectile



(d) 0.090-inch Stressed Specimen  
0.160-inch Shield, 1/4-inch Projectile

SCALE:  
1 Inch

Figure 24 EFFECT OF 2 INCHES OF Q-FELT INSULATION FILLER

**CONFIDENTIAL**

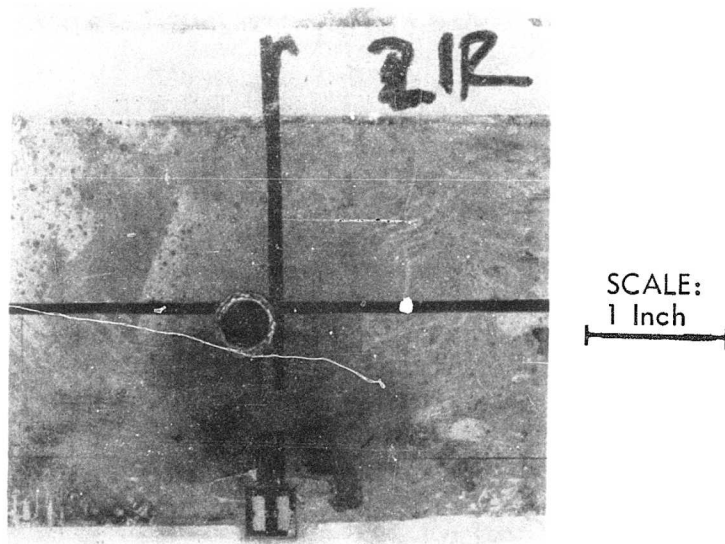
## CONFIDENTIAL

hole formed in the specimen was about the same as would be produced on the same specimen without a backing medium. None of these specimens were fractured, nor were any cracks formed. However, the pulse generated in the paraffin was sufficient to bulge the specimen in the area surrounding the penetration. The bulge, shown in Figure 25b, was 0.10 inch high and about 2 inches in diameter. The direction of the bulge was opposite to the projectile flight direction.

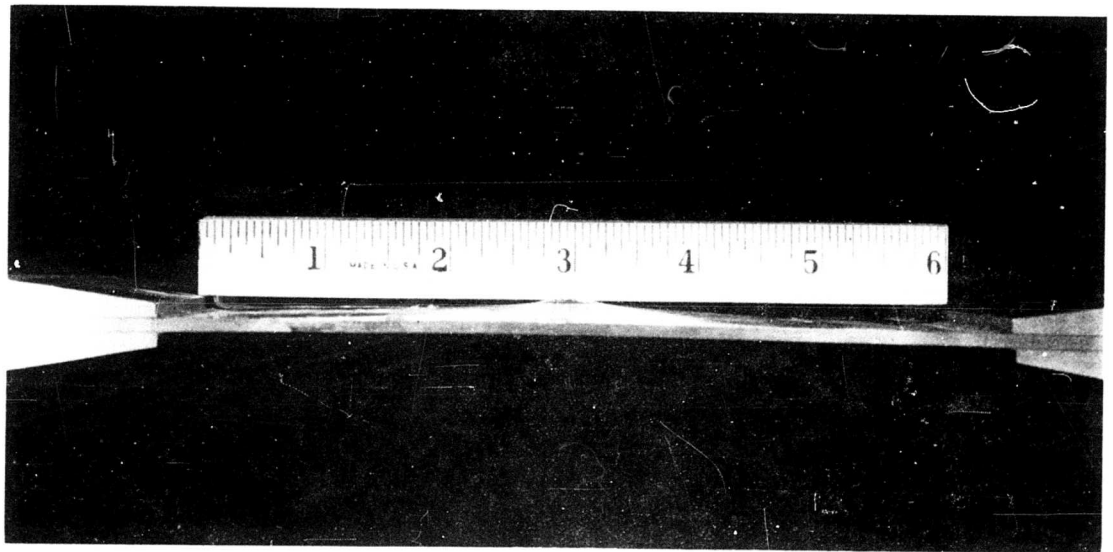
The 1/8-inch diameter projectile was not large enough to produce a crack-inducing pressure pulse, so another test was performed on a 0.090-inch specimen with a 1/4-inch diameter aluminum projectile. The results of the impact and subsequent effects, shown in Figure 26, were somewhat greater than expected. Figure 26b compares the fractured specimen to an untested specimen. The loose pieces have been taped in place for this photograph. The region of sharp curvature coincides with the top and bottom, respectively, of the testing jig beams. Damage to the paraffin backing blocks is shown in Figure 27. The test face of the block is 4 by 5 inches.

These tests, although exploratory in nature, have demonstrated the possible failure modes due to the shock interaction associated with the hypervelocity impact on pressure vessels containing liquids or solid propellants.

**CONFIDENTIAL**



(a) Impact Side of Hole



Projectile Flight Direction ↓

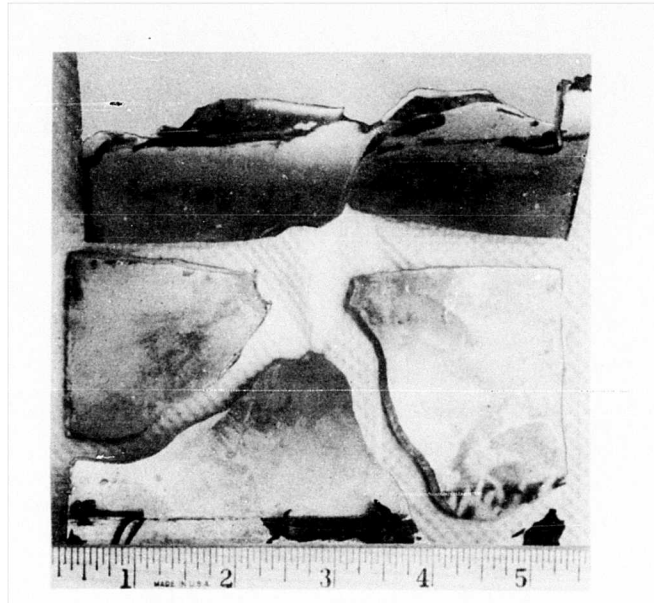
(b) Edge View Showing Upstream Bulge Formed by Impact and Subsequent Pressure Pulse

**Figure 25 EFFECT OF PARAFFIN BACKING ON IMPACT DAMAGE —  
1/8-INCH PROJECTILE**

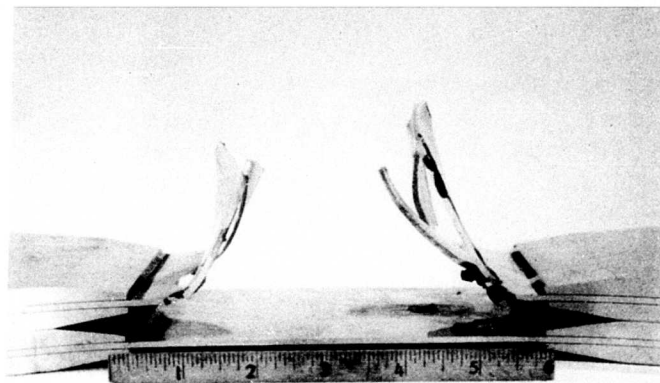
0.090-Inch 2014-T6 Specimen  
Static Stress 38,500 psi

**CONFIDENTIAL**

**CONFIDENTIAL**



(a) Exit Face of Specimen



(b) Edge View of Specimen

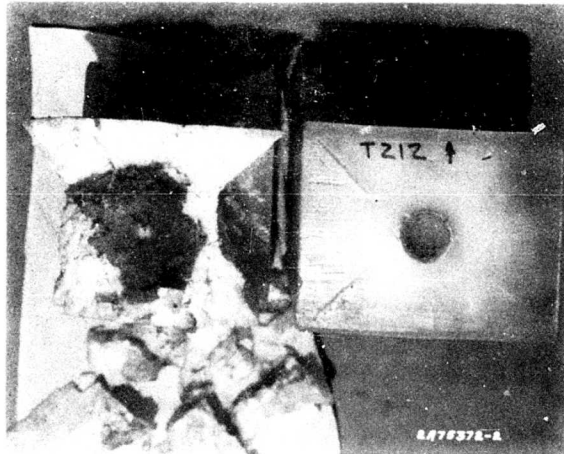
**Figure 26 EFFECT OF PARAFFIN BACKING ON IMPACT DAMAGE —  
1/4-INCH PROJECTILE**

0.090-Inch 2014-T6 Specimen  
Static Stress 48,100 psi

**CONFIDENTIAL**

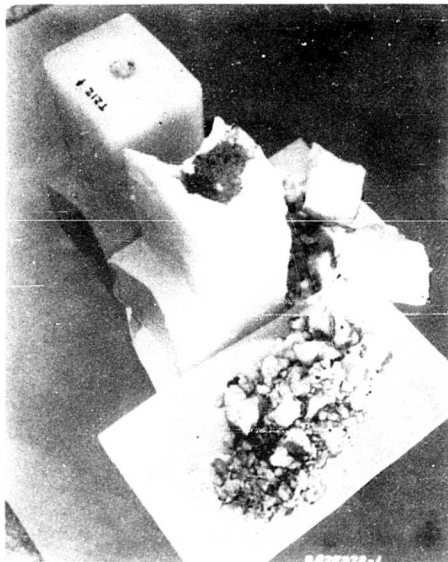


**CONFIDENTIAL**



(a) View of Craters  
1/4-Inch Projectile Test on Left  
1/8-Inch Projectile Test on Right

SCALE: 1 Inch  
└───┘



(b) View of Paraffin Blocks and Debris

**Figure 27 DAMAGE TO PARAFFIN BACKING BLOCKS  
AFTER PENETRATION OF 0.090-INCH 2014-T6 SPECIMENS**

**CONFIDENTIAL**

## CONFIDENTIAL

### VI. PHASE III TEST RESULTS

The Phase III tests are an exploratory investigation of the effect of projectile geometry on the penetration of practical structural arrangements of loaded thin sheets, with and without shields. The projectiles that have been tested are shown in Figure 28. These are an equilateral tetrahedron, a hollow cylinder, and a cupped cube. The projectiles are sized to fit within a 1/4-inch launch tube and to have the same mass as an 1/8-inch diameter sphere. The penetration data for the various shapes can be directly correlated with the corresponding Phase II tests previously discussed. The flight photographs displayed in Figure 29 were taken with Abtronics image-converter cameras. They show an 1/8-inch diameter sphere, an equilateral tetrahedron, and a hollow cylinder in flight immediately prior to impact, and a sphere and a cupped cube immediately subsequent to impact. Exposure time was 5 nanoseconds. The photograph of the cupped cube was taken before the projectile had time to disintegrate.

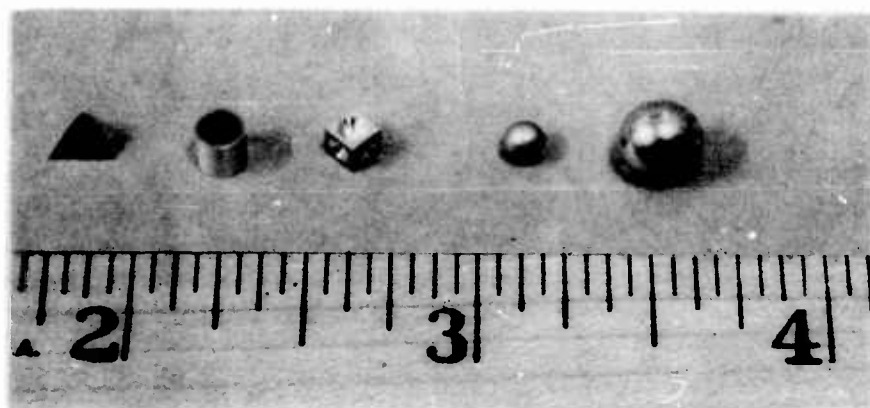
The Phase III tests that have been performed are listed in Table 3. The corresponding Phase II tests utilizing 1/8-inch diameter projectiles are also included for comparison. Typical results are shown in Figures 30, 31, and 32; the first shows craters formed in thick, unshielded stressed specimens, the second depicts penetration of thin unshielded targets, and the last is a compilation of the effects of various amounts of shielding. The unshielded stressed specimen was either 0.160 or 0.375 inch thick; the stressed specimen used for all shielded tests was 0.090 inch thick.

The tetrahedron projectile has exhibited a greater penetrating power than a sphere of equal mass. Craters formed in single sheets by the tetrahedron have smaller diameters, but are deeper; they tend to be more parabolic than hemispherical in shape. This is shown in Figure 30a-d. A tetrahedron impact sometimes forms triangular-shaped holes in thin sheets. Tetrahedrons have successfully penetrated stressed specimens protected with 0.090-inch shields. Spheres of the same mass and at the same velocity have penetrated stressed specimens only when the shield is less than 0.040 inch thick.

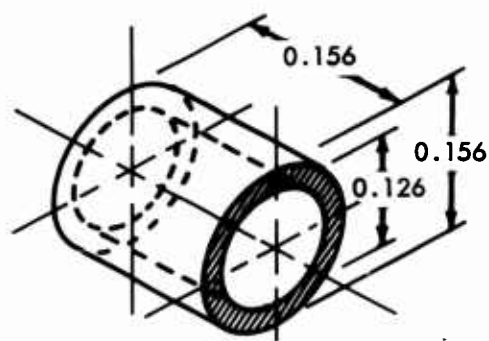
The tetrahedron is the only Phase III projectile that caused a specimen to fracture; a specimen tested with a 0.040-inch thick shield fractured while being removed from the jig. The removal procedure imposes a slight increase of stress on the specimen. A reasonable estimate of this additional stress, together with the apparent flaw size of 0.70 inch, indicates a fracture toughness value approaching 60 ksi  $\sqrt{\text{in}}$ . This is consistent with the values obtained from the Phase II tests of 2014-T6.

Depending upon projectile orientation at time of impact, the hollow cylinder can have a greater penetrating power than a sphere, but it is also more frangible. For the crater shown in Figure 30e and f, the cylindrical axis of the projectile was shown by the Abtronics camera to be within 10 degrees to the normal of the target. The raised point in the crater bottom coincides with the hole in the

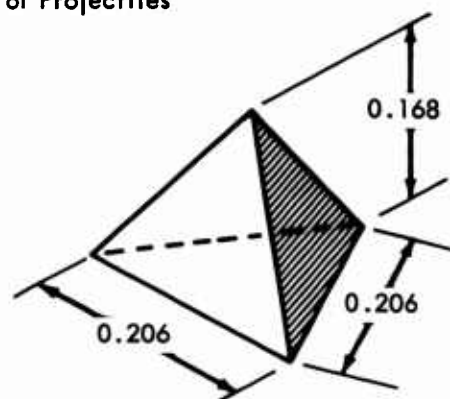
**CONFIDENTIAL**



(a) Photograph of Projectiles

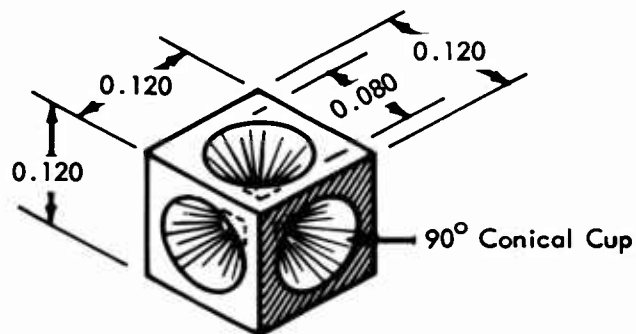


(b) Hollow Cylinder



(c) Equilateral Tetrahedron

Dimensions  
are in  
Inches



(d) Cupped Cube

**Figure 28 PROJECTILE GEOMETRY**

**CONFIDENTIAL**

CONFIDENTIAL

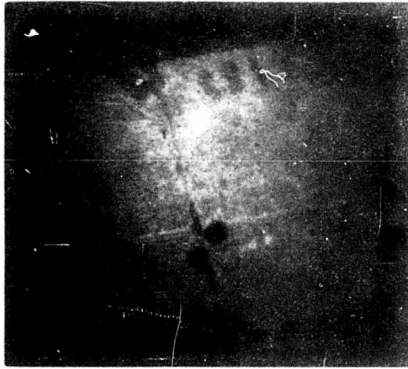
Test No.	STRESSED SPECIMEN				SHIELD			Type	PROJECTILE			FIG NO.	NOTES
	Width & Thick. (inches)	Matl Stress (psi)	Crater Dia (inches)	Damage Dia (inches)	Failure Mode	Thick. (inches)	Matl (inches)	Spacing (inches)	Filler Dia (inches)	Hole Dia (inches)	Matl Mass (grams)	Vel (fps)	
T-71	5 .160 2014-T6 45,800 P .36				NF								
T-143	5 .160 2014-T6 47,400 P .33				NF								
T-206	5 .160 2014-T6 47,300 P .32				NF								
T-51	5 .375 2014-T6 35,700 C .40				NF								
R-127	5 .375 2014-T6 36,000 C				NF								
T-129	5 .375 2014-T6 35,800 C .34				NF								
T-139	5 .375 2014-T6 36,000 C .32				NF								
T-117	5 .090 2014-T6 48,000 P .15	1.10			FR	.020	7075-T6	2		.19			
T-141	5 .090 2014-T6 47,500 P .28	.80			NF	.020	7075-T6	2		.20			
T-160	5 .090 2014-T6 46,500 P .26	.80			NF	.020	7075-T6	2		.23			
T-161	5 .090 2014-T6 48,700 P .25	.65			NF	.020	7075-T6	2		.20			
R-80	5 .090 2014-T6 48,200 C .05	2.00			NF	.040	2014-T6	2		.26			
T-95	5 .090 2014-T6 47,900 C .12	1.30			F	.040	2014-T6	2		.28			
R-180	5 .090 2014-T6 48,400 C .07	1.50			NF	.040	2014-T6	2		.23			
R-130	5 .090 2014-T6 47,900 P .15				F	.040	2014-T6	2		.25			
T-136	5 .090 2014-T6 47,800 P .12	.90			FR	.040	2014-T6	2		.26			
R-135	5 .090 2014-T6 48,200				NF	.040	2014-T6	2	Q-Felt				
T-140	5 .090 2014-T6 47,900 C .12	1.00			NF	.040	2014-T6	2		.28			
T-144	5 .090 2014-T6 47,750 C .14	1.20			NF	.040	2014-T6	2		.30			
T-78	5 .090 2014-T6 48,200 C .10	2.00			NF	.090	2014-T6	2		.35			
R-165	5 .090 2014-T6 46,900 C .08	1.50			NF	.090	2014-T6	2		.28			
R-166	5 .090 2014-T6 48,000 C .09	1.50			NF	.090	2014-T6	2		.28			
R-168	5 .090 2014-T6 48,000 C .12	2.25			NF	.090	2014-T6	2					
T-204	5 .090 2014-T6 48,400 P .10	2.00			NF	.090	2014-T6	2		.32			
T-207	5 .090 2014-T6 48,300 P .10	1.75			NF	.090	2014-T6	2		.35			
R-208	5 .090 2014-T6 48,500 P .11	1.75			NF	.090	2014-T6	2		.25			
T-81	5 .090 2014-T6 47,300 C .11	1.50			NF	.160	2014-T6	2		.31			
T-236	5 .090 2014-T6 47,900 C .10	1.30			NF	.160	2024-T3	2		.30			
R-237	5 .090 2014-T6 48,400 C .09	1.75			NF	.160	2024-T3	2		.35			

P = Complete Penetration  
 C = Crater, No Penetration  
 F = Specimen Fractured During Impact Event  
 NF = Specimen Did Not Fracture  
 FR = Specimen Fractured While Being Removed From the Jig  
 SP = Spherical Projectile  
 T = Tetrahedron Projectile  
 HC = Hollow Cylinder Projectile  
 CC = Cupped Cube Projectile  
 6 = Projectile Broke Up  
 13 = Sabot Impacted Target

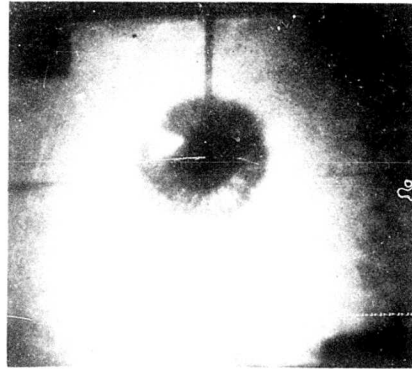
TABLE 3 - PHASE III TESTS  
Including Phase II Comparison Tests

CONFIDENTIAL

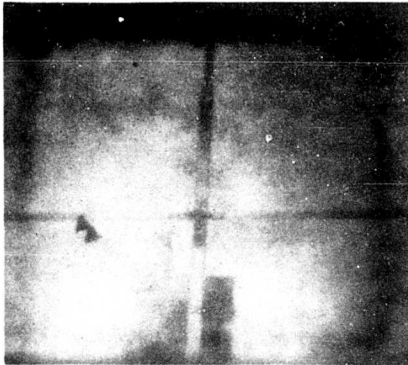
**CONFIDENTIAL**



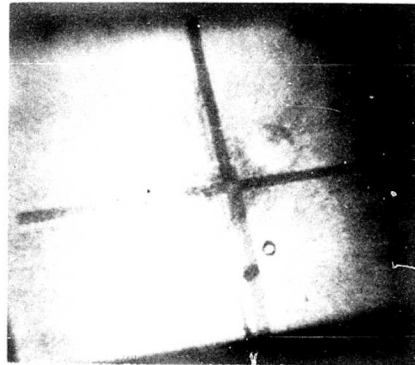
(a) 1/8-Inch Sphere Immediately Prior to Impact.  
Note Projectile Shadow.



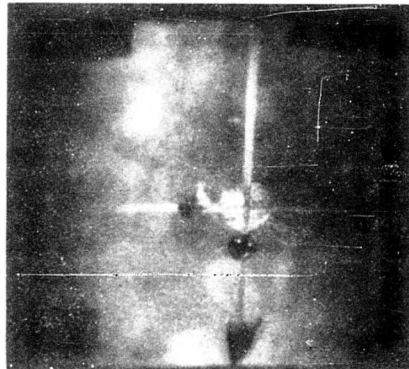
(b) 1/8-Inch Sphere Immediately After Impact.



(c) Tetrahedron Immediately Prior to Impact.  
Note Projectile Shadow.



(d) Hollow Cylinder Immediately Prior to Impact.  
Note Projectile Shadow.



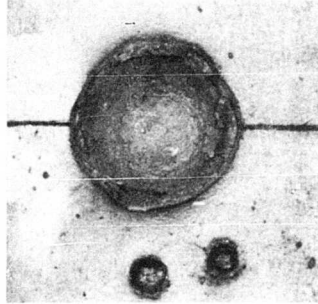
(e) Cupped Cube Immediately After Impact.

Figure 29 PROJECTILES IN FLIGHT

**CONFIDENTIAL**

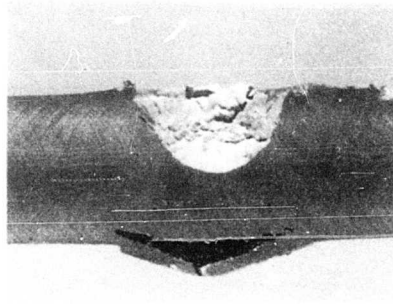
**CONFIDENTIAL**

SCALE:  
1/2 Inch

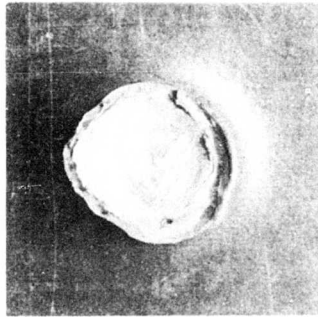


(a) Crater  
1/8-Inch Sphere - 0.05 grams

SCALE:  
1/2 Inch



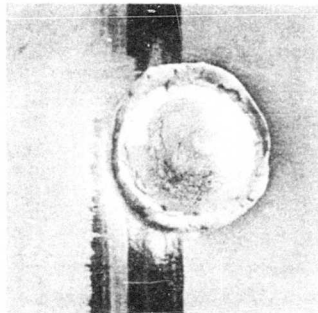
(b) Section



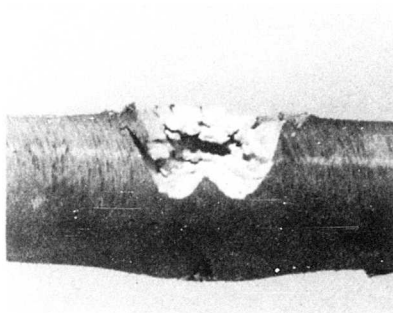
(c) Crater  
Tetrahedron - 0.049 grams



(d) Section



(e) Crater  
Hollow Cylinder - 0.047 grams



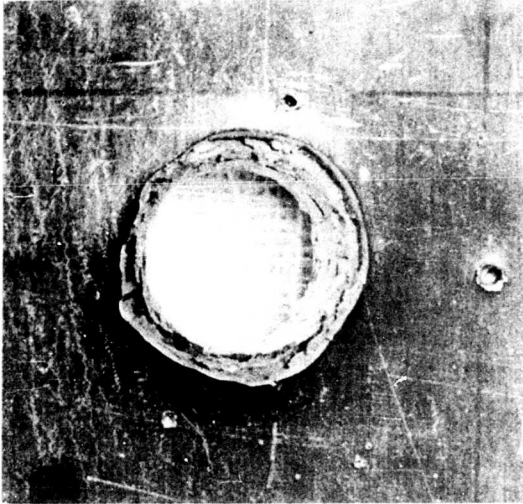
(f) Section

**Figure 30 EFFECT OF PROJECTILE GEOMETRY -  
CRATERS IN UNSHIELDED SPECIMENS**

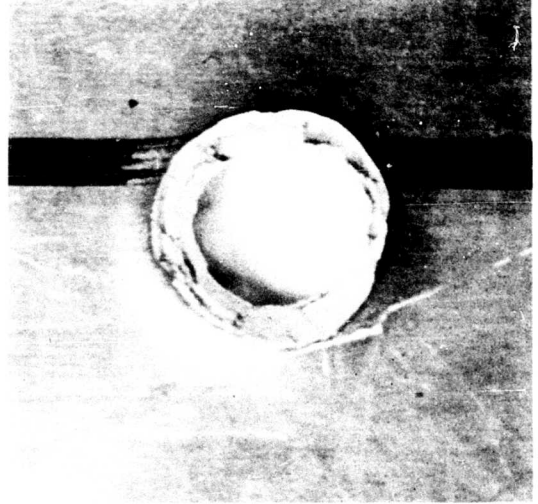
0.375-Inch 2014-T6 Specimens  
Static Stress 36,000 psi

**CONFIDENTIAL**

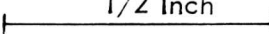
**CONFIDENTIAL**

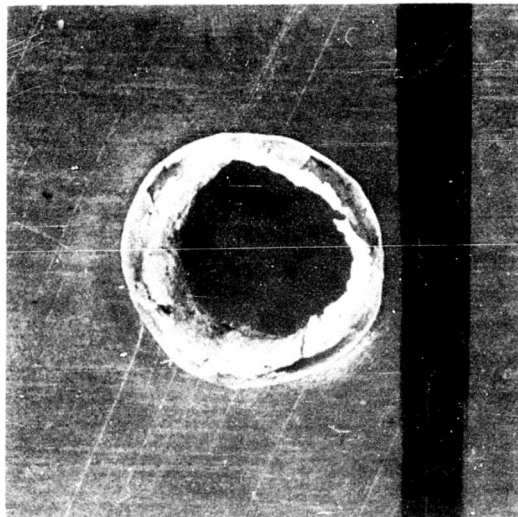


(a) 1/8 Inch Sphere - 0.05 Grams



(b) Tetrahedron - 0.049 Grams

SCALE:  1/2 Inch



(c) Hollow Cylinder - 0.044 Grams

**Figure 31 EFFECT OF PROJECTILE GEOMETRY - PENETRATIONS  
IN UNSHIELDED SPECIMENS**

0.160-inch 2014-T6 Specimens

Static Stress 48,000 psi

**CONFIDENTIAL**

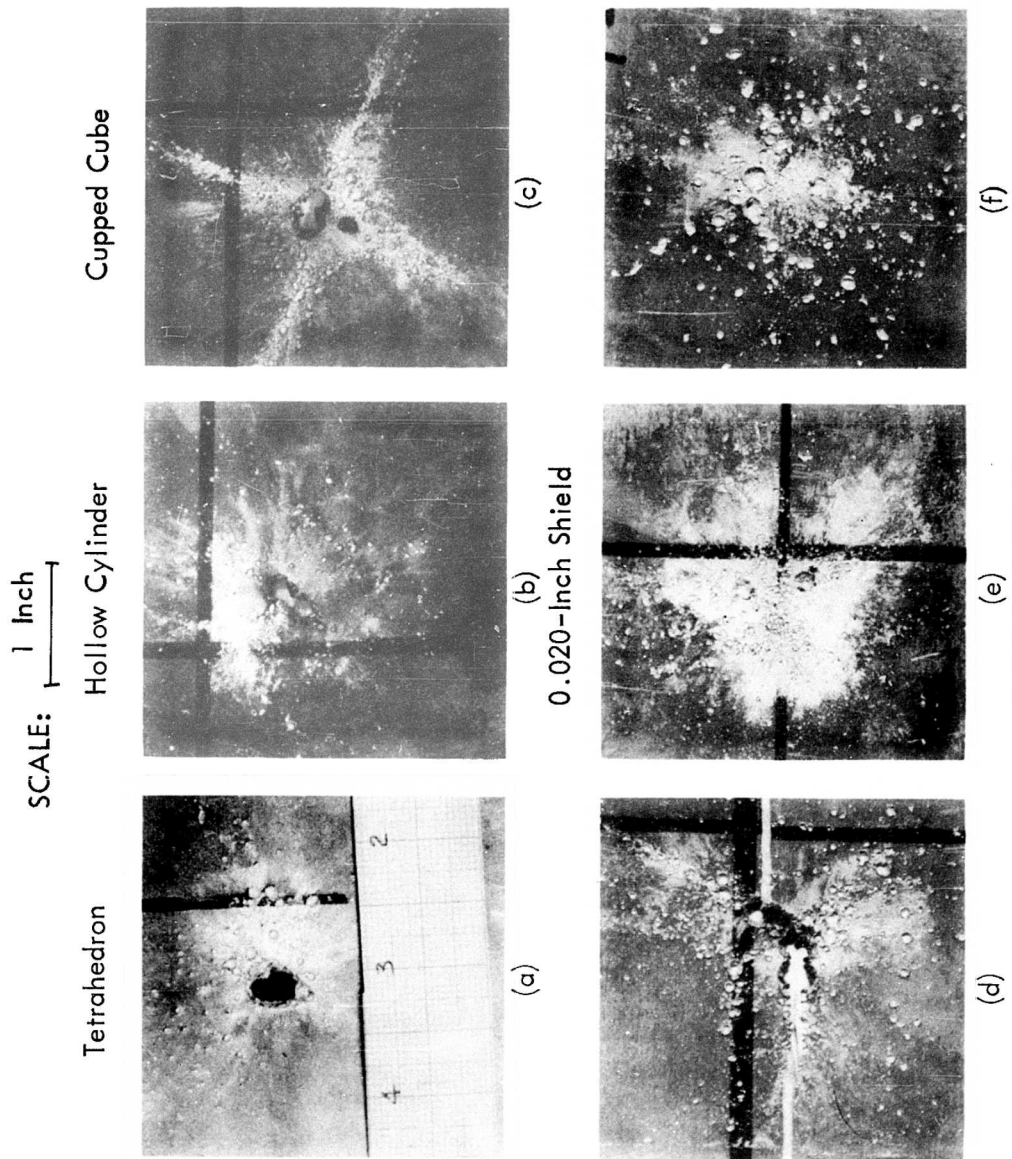


Figure 32 EFFECT OF PROJECTILE GEOMETRY AND SHIELD THICKNESS

0.090-Inch 2014-T6 Specimens 2-Inch Shield Spacing  
Static Stress 48,000 psi



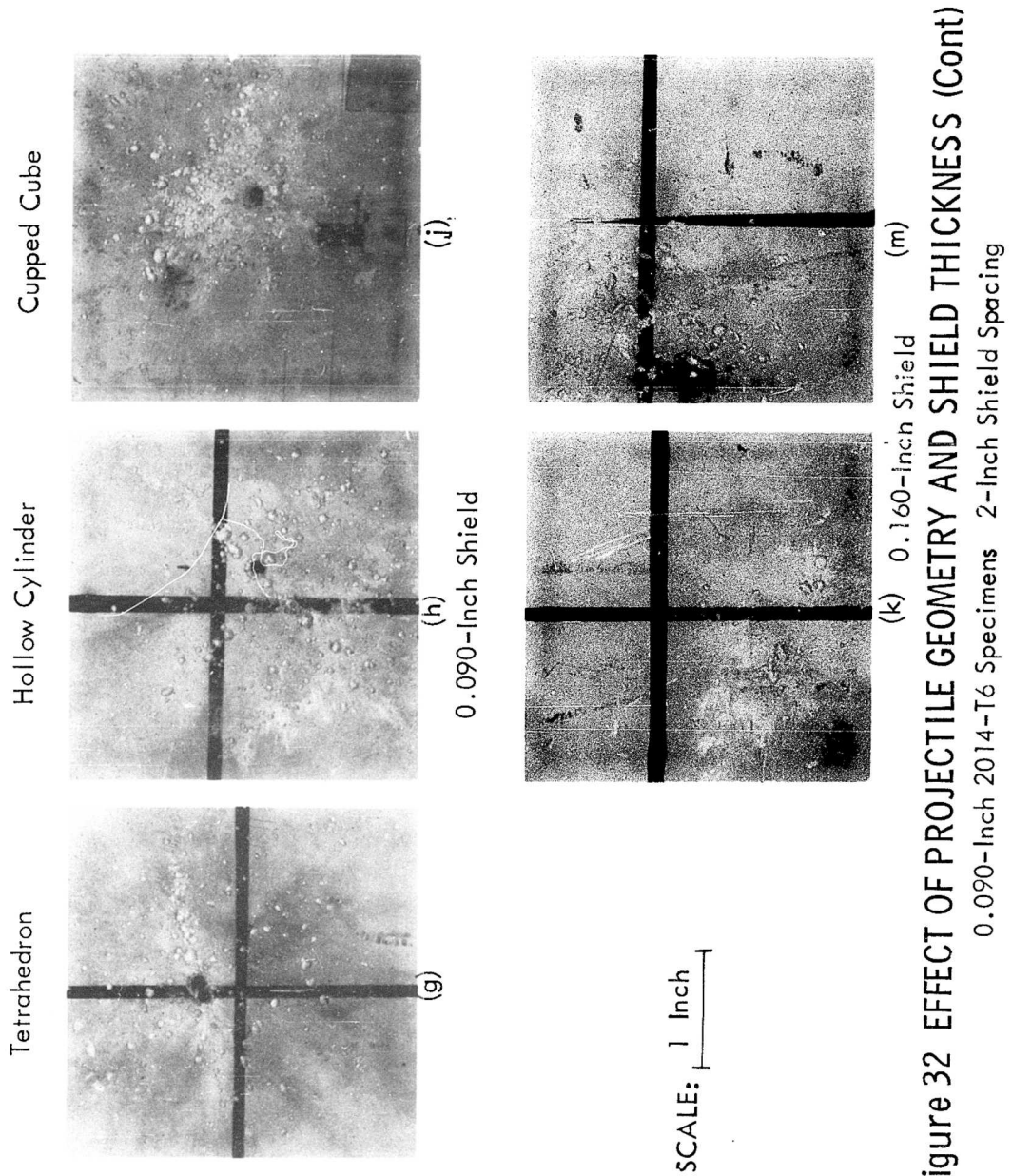


Figure 32 EFFECT OF PROJECTILE GEOMETRY AND SHIELD THICKNESS (Cont)

## CONFIDENTIAL

cylinder. When the cylindrical axis is parallel to the plane of the target, the projectile breaks up easier and produces less penetration. In the test shown in Figure 32h, where the hollow cylinder penetrated both the shield and the stressed specimen, the axis was normal to the plane of the sheet.

The cupped cube was tested against shielded specimens only. The impact attitude of this projectile also has an effect on subsequent behavior. A characteristic pattern produced by this projectile is displayed in Figure 32c. The Abtronics photographs of the impact of this projectile show that the projectile had one face parallel to the shield and the other faces oriented so that the diagonals of the cube coincide with the line of craters on the second sheet.

The results of the hollow cylinder tests are comparable to that reported in Reference 6. The tetrahedron and cupped cube tests are believed to be the first time such shapes have been fired as hypervelocity projectiles. No previous experimental programs have studied the effect of projectile geometry on impact of stressed specimens. Although the Phase III tests were performed as an exploratory investigation with limited parameter variations, some interesting results have been obtained. In particular, crater shape and hole size are affected by projectile geometry. This suggests the possibility of tailoring a projectile to the characteristics of the target. A cupped cube projectile, for example, that distributes craters in long lines on shielded targets may more readily induce catastrophic failure than the same mass in the form of a rod or sphere.

## CONFIDENTIAL

### VII. PHASE IV TEST RESULTS

Prediction of the conditions under which a pressure vessel will fail due to hypervelocity impact requires confirming tests using pressurized tanks as test specimens. The Phase IV test series has been designed to accomplish this result. The impact conditions that produced failures for the uniaxially loaded screening specimens have been duplicated in Phase IV tests. This permits the effect of biaxial stress on structural response and fracture modes to be determined. In addition, the significance of screening specimen geometric limitations, e.g., specimen curvature and width, can be evaluated.

Table 4 summarizes the results of Phase IV tests. Test results are described below. The stresses reported are based on a nominal wall thickness of about 0.102 inch; actual values will be measured later.

#### Unshielded Air-Pressurized Tanks

The screening tests of a projectile impacting an unshielded, stressed 2014-T6 specimen indicate the material will suffer a penetration but will not fracture due to impacts of 0.38-gram projectiles at velocities of 16,000 feet per second. Two Phase IV tests have been performed to determine if biaxially stressed specimens offer different responses. For the first of these, an 11-inch diameter 2014-T6 spherical tank with 0.100-inch thick walls was impacted by an 1/8-inch aluminum sphere. The resulting penetration, shown in Figure 33a, was a hole 0.35 inch in diameter. This is the same size as obtained from the uniaxially loaded specimen under similar impact conditions. A 22-inch diameter 2014-T6 spherical tank was impacted by a 1/4-inch aluminum projectile. The hole formed is shown in Figure 33c. The increased size of this hole, e.g., 0.70-inch diameter against 0.53 inch for the uniaxially loaded specimens, Figure 33d, may be due to the tank wall being thicker than the screening specimen. There were no signs of stress-induced differences in the penetrations of either tank.

This last test produced an interesting sidelight. Before the test, the tank had been filled with expanded mica to prevent the projectile or spall fragments from damaging the back tank wall following initial penetration. The mica performed as planned, effectively stopping the projectile and spall fragments; however, the mica was also pulverized during the test, and was ejected from the test tank through the penetration hole by the pressurizing air. The mica dust escaped directly into the testing laboratory as a thick brown smoke. Visibility was reduced to about 3 feet. When the smoke cleared, the test range appeared as shown in Figure 34. The laboratory ceased operation for 24 hours to clean house.

#### Shielded Air-Pressurized Tanks

Several air-pressurized tank tests using shields have been performed. Photographs of these tests and comparable uniaxially loaded shielded specimens are shown in Figure 35. The first of the shielded tank tests was with an 1/8-inch diameter projectile and an 0.040-inch shield. It was anticipated that the specimen

CONFIDENTIAL

PRESSURE VESSEL										SHIELD			PROJECTILE			FIG NO.	PHASE I/TEST	NOTES	
Test No.	Tank Dia (inches)	Matl	Stress (psi)	Crater Dia (inches)	Damage Dia (inches)	Failure Mode	Tank Content	Pressure (psia)	Thick. (inches)	Matl	Spacing (inches)	Hole Dia (inches)	Type Dia (inches)	Matl	Mass (grams)	Vel (fps)			
T-132	11.09	2014-T6	47,500	P .35		NF	Air	1782					SP	1/8	Al	.05	15,333	33	T-77
R-174	11.09	2014-T6	38	P .31		FC	Water	14					SP	1/8	Al	.05	15,936	36	13,14
T-320	22.5.8	2014-T6	43,700	P .70		NF	Air	794					SP	1/4	Al	.38	16,133	33,34	T-150
T-330	22.5.8	2014-T6	77	P .66		FC	Water	14					SP	1/4	Al	.38	15,966	36	15
T-336	22.5.8	2014-T6	77	P .15	.60	NF	Water	14	.010	7075-T6	2	.15	SP	1/8	Al	.05	15,080	37	
R-323	22.5.8	2014-T6	43,700	P .49	.70	NF	Air	794	.020	7075-T6	2	.31	SP	1/8	Al	.05	15,106	35	T-117
T-335	22.5.8	2014-T6	77	C .14	.80	NF	Water	14	.020	7075-T6	2	.19	SP	1/8	Al	.05	15,700	37	
T-322	22.5.8	2014-T6	43,700	C .09	1.15	NF	Air	794	.040	2014-T6	2	.24	SP	1/8	Al	.05	15,056	35	R-80,T-95
T-332	22.5.8	2014-T6	77	C .12	1.50	NF	Water	14	.040	2014-T6	2	.32	SP	1/8	Al	.05	14,746	37	R-180
T-337	22.5.8	2014-T6	0	P .40	1.80	NF	Air	0	.160	2024-T3	2	.68	SP	1/4	Al	.38	14,955	35	T-158

CONFIDENTIAL

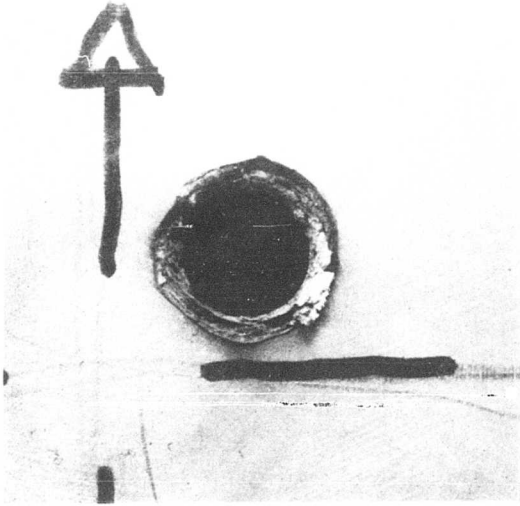
TABLE 4 - PHASE IV TESTS

P = Complete Penetration  
 C = Crater, No Penetration  
 NF = Specimen Did Not Fracture  
 FC = Specimen Suffered a Major, Critical Crack Due to Impact

SP = Spherical Projectile  
 13 Sabot Impacted Target  
 14 Total Crack Length 21 Inches  
 15 Total Crack Length 24 Inches

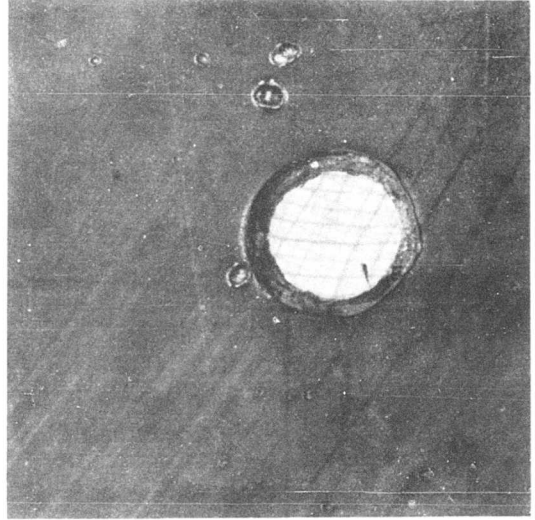
**CONFIDENTIAL**

Air-Pressurized Tanks



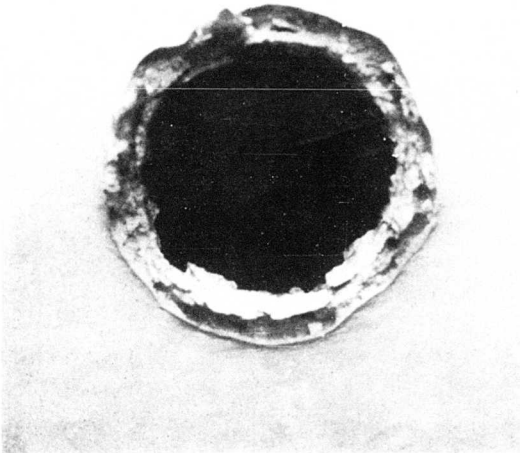
(a) 11-Inch-Diameter Tank  
Static Stress 47,500 psi

Uniaxially Stressed Specimen

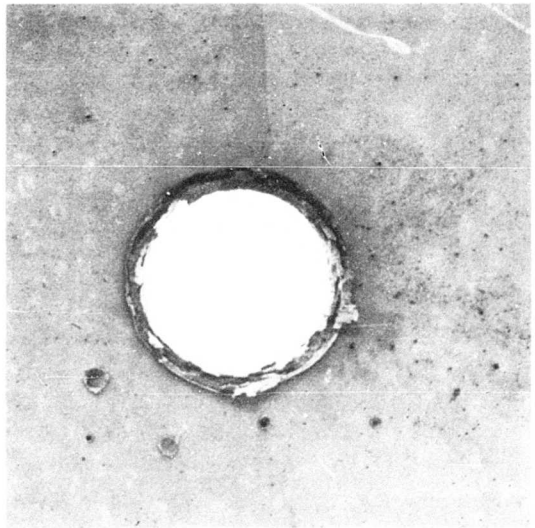


(b) Static Stress 47,000 psi

1/8-Inch Aluminum Sphere Projectile SCALE:  $\frac{1}{2}$  Inch



(c) 22-Inch-Diameter Tank  
Static Stress 43,700 psi



(d) Static Stress 48,300 psi

1/4-Inch Aluminum Sphere Projectile

**Figure 33 COMPARISON OF UNSHIELDED TESTS  
OF UNIAXIAL AND BIAXIAL SPECIMENS**

**CONFIDENTIAL**

CONFIDENTIAL

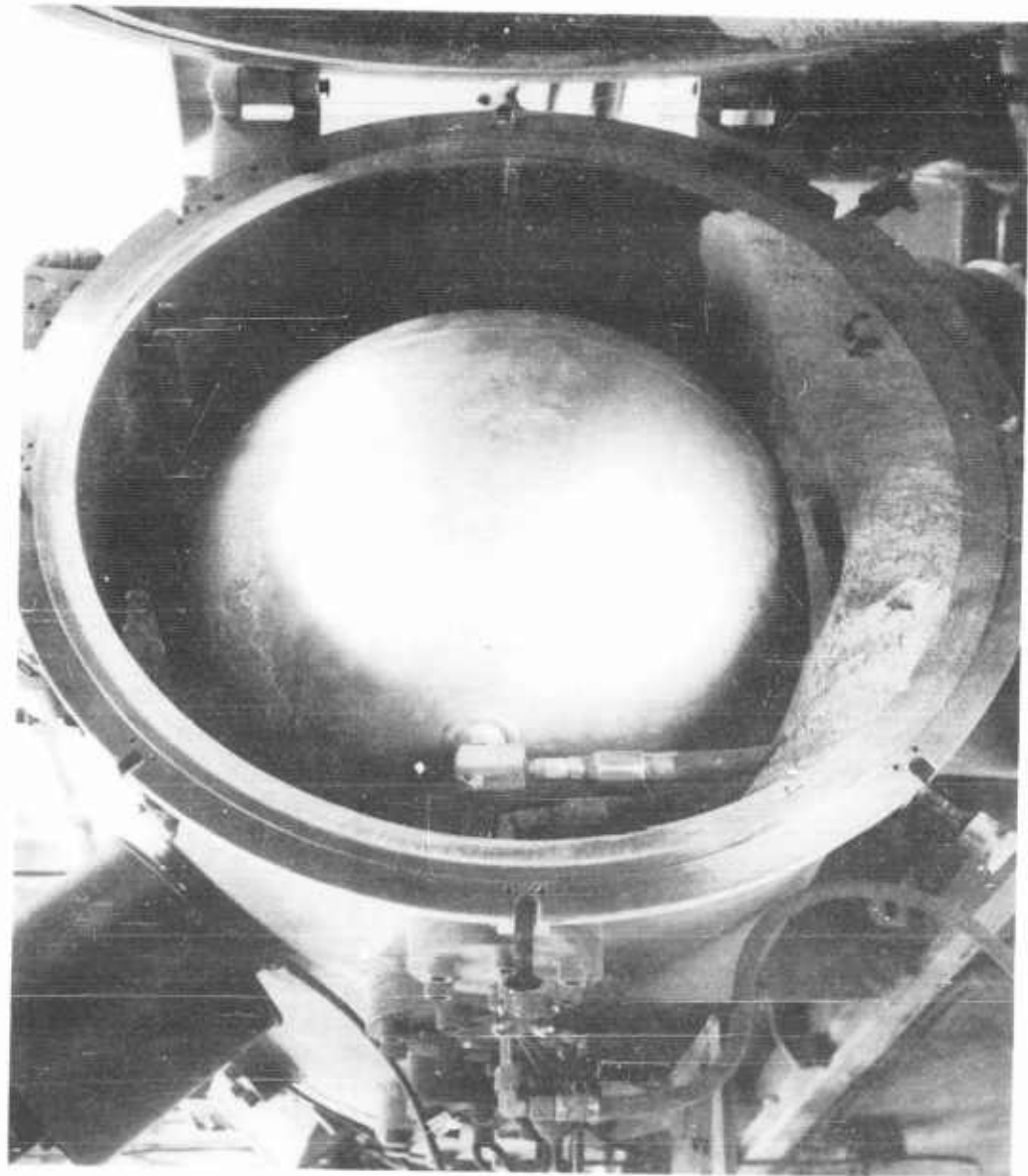
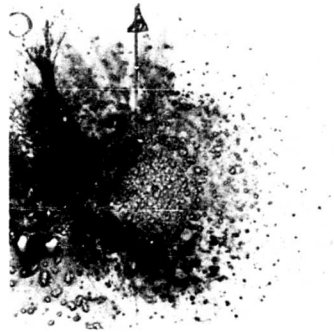
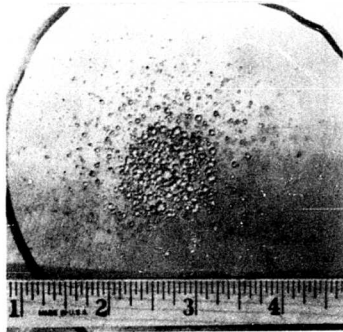


Figure 34 LIGHT-GAS GUN RANGE AND TANK SPECIMEN

CONFIDENTIAL

Air-Pressurized Tank  
(22-Inch Diameter)

Uniaxially Stressed Specimen

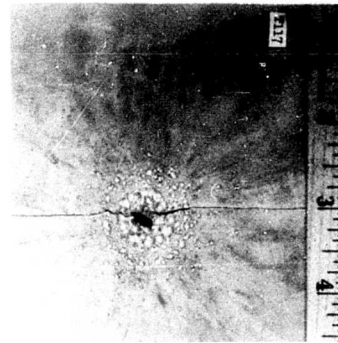
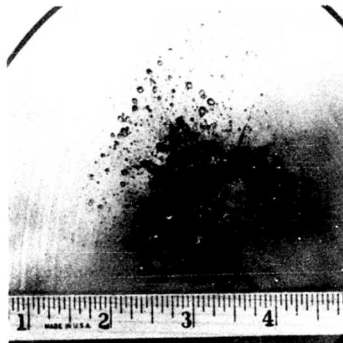


Sabot  
Impact  
On Left

(a) Static Stress 43,700 psi  
0.040-Inch Shield - 1/8-Inch Projectile

(b) Static Stress 48,400 psi  
0.040-Inch Shield - 1/8-Inch Projectile

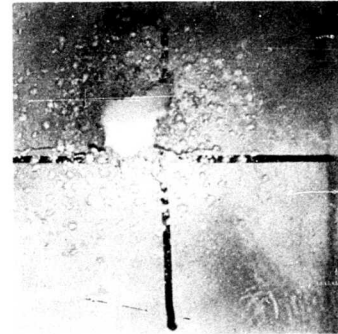
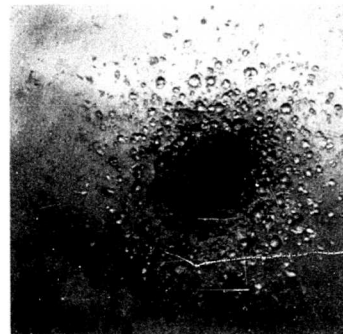
Sabot  
Impact  
Center



SCALE:  
1 Inch

(c) Static Stress 43,700 psi  
0.020-Inch Shield - 1/8-Inch Projectile

(d) Static Stress 48,000 psi  
0.020-Inch Shield - 1/8-Inch Projectile



(e) Static Stress 0 psi  
0.160-Inch Shield - 1/4-Inch Projectile

(f) Static Stress 0 psi  
0.160-Inch Shield - 1/4-Inch Projectile

Figure 35 COMPARISON OF SHIELDED TESTS  
OF UNIAXIAL AND BIAXIAL SPECIMENS

## CONFIDENTIAL

would sustain surface damage from many small craters, but would not fracture. The result, shown in Figure 35a, was a multitude of craters within a 1.15-inch diameter area. This compares favorably with the same test configuration using the uniaxially stressed specimen shown in Figure 35b.

The next test used an 1/8-inch diameter projectile and an 0.020-inch shield. The comparable screening specimen test sustained impact without fracture, but broke when the static load was increased during removal from the jig. This indicates the 1/8-inch projectile to be marginal for producing fracture under the given conditions. If a biaxial stress field were more detrimental, a tank specimen tested under these conditions should fracture. The results are shown in Figures 35c and 35d. The difference in response is due to sabot impact. The test, however, did prove the 0.70-inch damage diameter is not critical for this particular shielded pressure vessel configuration.

The shielded tank test shown in Figure 35e duplicated the same test parameters that were used for the Phase II screening tests where the large deformations and cracks resulted, i. e., a 1/4-inch aluminum projectile and a 0.160-inch thick shield impacting unstressed specimens. The gross deformation and critical cracking common to the uniaxial specimens did not occur for the tank specimen. The area immediately adjacent to the penetration suffered only a 0.1-inch deflection from the original surface. The tank wall thickness has not yet been measured. It may be significantly thicker than the screening specimens; this is sufficient to explain the difference in response.

### Water-Filled Tanks

Tests reported elsewhere (Reference 7) indicate that catastrophic fracturing rather than simple puncturing of pressure vessels may occur when they are filled with liquids and impacted by a hypervelocity projectile. To investigate this phenomenon, impact tests of water-filled tanks were performed. To distinguish the effect of water from that of static stress, tank tests were made without pressurization. The pressure pulse generated by the impact shock in the water is presumed to be the primary factor in producing catastrophic fracture. This reasoning is supported by the results obtained from the paraffin-backed screening tests. In these tests a 1/4-inch aluminum projectile produced fracture of the specimen, but the 1/8-inch projectile did not. Figure 36 shows the failures of unshielded, unstressed, water-filled tanks of two different sizes. Both tanks suffered catastrophic cracks. The first, in an 11-inch diameter tank, was due to an 1/8-inch aluminum projectile and two sabot fragments; the second, in a 22-inch diameter tank, was due to a 1/4-inch aluminum projectile. Crack length in both cases was over 20 inches. The pressure pulses generated in the liquid were also large enough to bulge the tank outward near the area of the penetration.

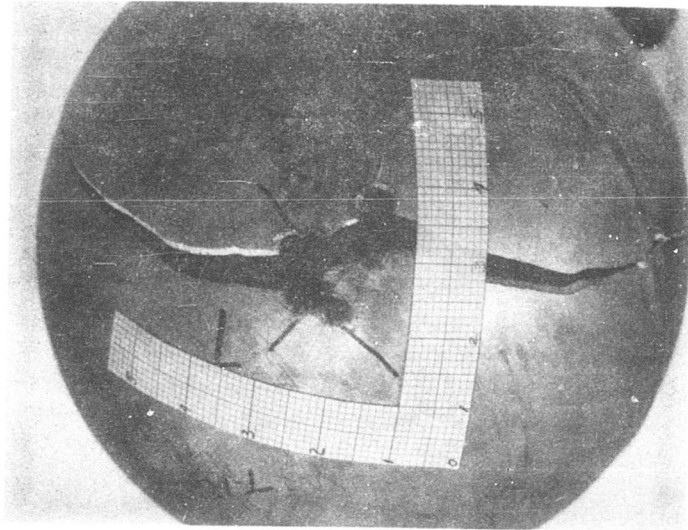
It is also of interest to investigate shielding effects, where the water-filled tank is not necessarily penetrated, but the damage is distributed over a larger area due to projectile dispersion. Figure 37 shows the results of three shielded,



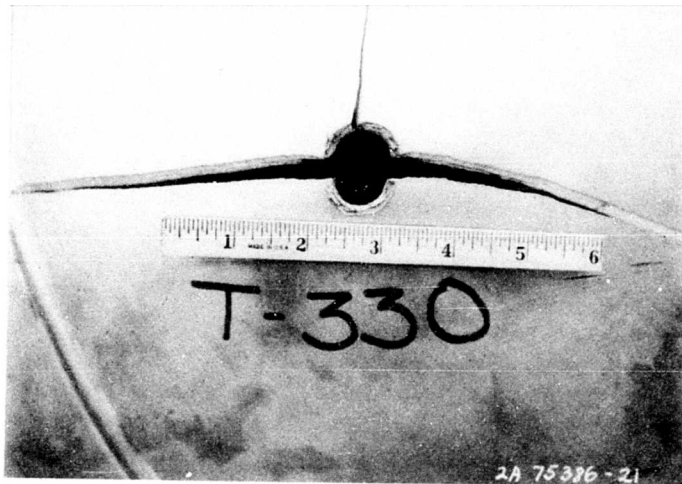
**CONFIDENTIAL**

unstressed, water-filled tank tests employing 1/8-inch diameter aluminum projectiles. Although considerable surface damage has been done to the tank wall, no fracture or crack was produced under the interaction of the impact and the water inside the tank. In one test using an 0.010-inch shield, as shown in Figure 37c, the projectile perforated the tank; the spall remained attached so that little or no material entered the tank. No through-the-thickness cracks were formed in this test.

**CONFIDENTIAL**



(a) 11-Inch-Diameter Tank  
1/8-Inch Projectile Plus Sabot



(b) 22-Inch-Diameter Tank  
1/4-Inch Projectile

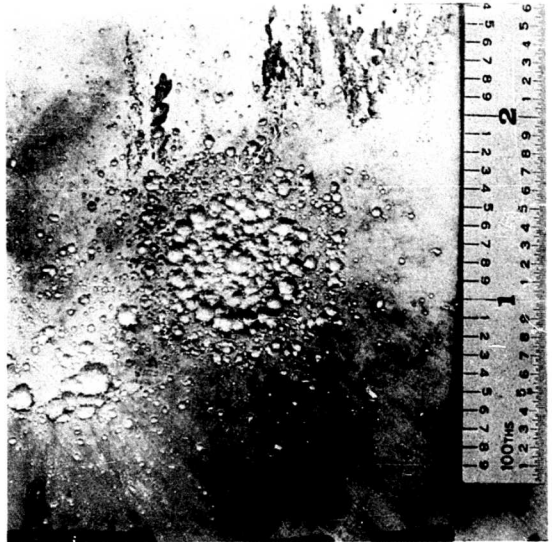
**Figure 36** IMPACT DAMAGE OF UNSHIELDED, WATER-FILLED TANKS  
Tank Pressure 15 psi

**CONFIDENTIAL**

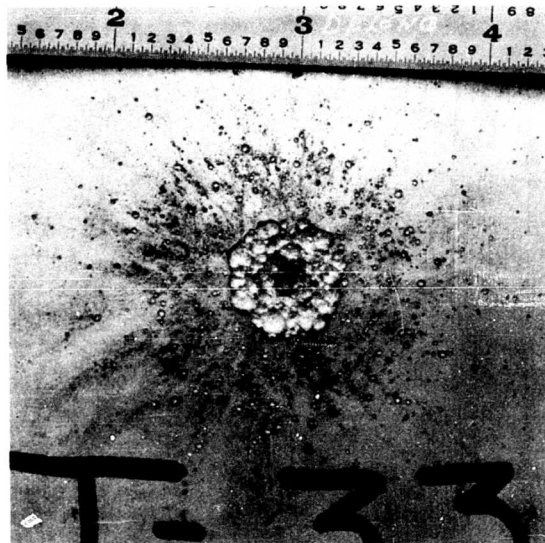
**CONFIDENTIAL**



(a) 0.040-Inch Shield  
Sabot Impact



(b) 0.020-Inch Shield



(c) 0.010-Inch Shield  
Tank Barely Penetrated

SCALE:  
1 Inch

**Figure 37 IMPACT DAMAGE OF SHIELDED, WATER-FILLED TANKS**

Tank Pressure 15 psi , 2-Inch Shield Spacing  
22-Inch-Diameter Tanks, 1/8-Inch Projectiles

**CONFIDENTIAL**

## CONFIDENTIAL

### VIII. CONCLUSIONS

Based on the results obtained from the four-phase experimental program given in this report, the following conclusions may be drawn:

- 1) There is no distinguishable change in crater configuration or hole size due to hypervelocity impact of specimens preloaded to various static stress levels. If transient impact stresses do not persist long enough for the material to respond, then only static stress systems need be considered in evaluation of failure modes. The crater or the hole generated may be treated as a stress concentration or flaw; the seriousness of the stress-concentration effect depends on the stress level as well as the material behavior.
- 2) Fracture failures may occur under hypervelocity impact at static stresses far below the material strength. Fracture mechanics, based on flaw-size and stress-field concepts, has been found useful in predicting structural failures under static and fatigue loadings. Although the flaw shape and conditions of loading under hypervelocity impact do not fulfill the analytical conditions of fracture mechanics, test results demonstrate that a limiting stress as a function of crater size exists. Both plane-stress and plane-strain fracture modes have been produced in aluminum specimens. The plane-stress mode is the shear-separation failure typical of thin sheets; the plane-strain mode is typical of thick-sheet failure where elastic constraint restricts shear-separation. Plane-stress fracture toughness values due to hypervelocity impact appear to agree with that predicted by static tests; plane-strain values obtained from impact tests of both aluminum and steel specimens have been higher than that predicted by static tests.
- 3) No fracture occurred for unshielded 2014-T6 aluminum sheet specimens subjected to hypervelocity impact at a static stress of 80 percent of material nominal yield strength. The hole in the stressed sheet did not approach the critical crack size for fracture; however, the addition of shields increased the damaged region to a size sufficient to produce fracture.
- 4) For the hypervelocity impact conditions used in this study, the relationship between the hole size and the target thickness for unshielded specimens, either with or without static stress, can be depicted by a single curve. For shielded targets, no such curve has yet been found.
- 5) The effect of varying shield thickness has been shown to produce complex damage-pattern changes on the shielded targets. Instead of giving protection, the use of a shield may, under certain conditions, serve to increase the damage capability of the projectile.
- 6) The use of an insulation material as a filler placed between the shield and the target may, under certain conditions, reduce the damage to the target produced by a hypervelocity projectile.

## CONFIDENTIAL

- 7) Equal-mass projectiles in the shape of tetrahedrons, cupped cubes, hollow cylinders, and spheres have been fired into shielded and unshielded specimen. Tetrahedrons and properly oriented hollow cylinders have exhibited greater penetration capabilities than equivalent spheres. In general, crater configuration follows the shape and orientation of the projectile in contact with the target.
- 8) There are no noticeable changes in hole size or crater configuration due to hypervelocity impact between biaxially loaded tanks and uniaxially loaded specimens of equal thickness. The effect of curvature has also been shown to be negligible.
- 9) Tests on specimens with paraffin backing show that catastrophic failure can occur. Failure is presumably due to the shock pressure generated in the paraffin block under hypervelocity impact. It is anticipated that hypervelocity impact on pressure vessels containing liquids or solid propellants will result in similar phenomena.
- 10) Impact tests on water-filled unstressed tanks have produced catastrophic fractures. The pressure pulse generated in the water is presumed to be the primary factor in producing failure.

Further testing is planned to support the evaluation of hypervelocity impact failure modes for pressure vessels. This includes the following work:

- 1) Additional shielded and unshielded stressed specimens will be tested to extend the applicability of static fracture mechanics concepts to hypervelocity impact damage analysis.
- 2) A series of tests will be performed to obtain quantitative information on pressure pulse impingement immediately subsequent to hypervelocity projectile penetration.

## IX. REFERENCES

1. Lee, D. H., and J. F. Lundeborg, "Impact Failure of Pressure Vessels," (Confidential), ASD-TDR-63-13, ASTIA AD-334641, The Boeing Company, April 1963
2. Barone, F. J., and A. M. Hall, "A Discussion of the Fracture Toughness of Several Stainless Steels in Sheet Form," DMIC Memorandum 164, Battelle Memorial Institute, Columbus, Ohio, January 1963
3. Anon., "Fracture Testing of High-Strength Sheet Materials," (Third Report of a Special ASTM Committee), Materials Research and Standards, ASTM, Vol. 1, No. 11, November 1961
4. Irwin, G. R., "Relation of Crack-Toughness Measurements to Practical Applications," ASME 62-MET-15, Paper presented at the AWS-ASME Metals Engineering Conference, Cleveland, Ohio, April 9-13, 1962
5. Maiden, C. J., "Investigation of Fundamental Mechanism of Damage to Thin Targets by Hypervelocity Projectiles," TM 63-201, GM Defense Research Laboratories, Santa Barbara, California, March 1963
6. Dittrich, W. H., et al., "Lethality of Hollow Shapes" (Secret), ASD-TDR-63-19, Oct. 4, Aeronautical Systems Division, Eglin Air Force Base, Florida, May 1963
7. Stepka, F. S. and C. R. Morse, "Preliminary Investigation of Catastrophic Fracture of Liquid-Filled Tanks Impacted by High-Velocity Particles," NASA TN D-1537, National Aeronautics and Space Administration, May 1963

# INITIAL DISTRIBUTION

1 DIRECTOR OF DEFENSE RESEARCH & ENGINEERING  
WASHINGTON 25, DC

ADVANCED RESEARCH PROJECTS AGENCY  
ROOM 2B-263 PENTAGON  
WASHINGTON 25, DC

1 MR BLOWER  
3 MR KOETHER

1 WEAPON SYSTEM EVALUATION GROUP  
ROOM 1E880, PENTAGON  
WASHINGTON 25, DC

Hq USAF  
WASHINGTON 25, DC

1 AFORQ-QT  
1 AFOCE  
1 AFCIN  
1 AFRDP  
1 AFRSTB  
1 AFRSTE

AIR FORCE SYSTEMS COMMAND  
ANDREWS AF BASE  
WASHINGTON 25, DC

1 SCTR  
1 MSFA  
1 SCSA

AERONAUTICAL SYSTEMS DIVISION  
WRIGHT-PATTERSON AF BASE, OHIO

1 ASNXR  
1 ASORC  
1 ASRCP  
1 ASRNG  
1 ASRCEA  
2 ASRMDS-21

FOREIGN TECHNOLOGY DIVISION  
WRIGHT-PATTERSON AF BASE, OHIO

2 TDCE  
1 TDBTL  
2 FT4E2  
1 TDEWA

SPACE SYSTEMS DIVISION  
AF UNIT POST OFFICE  
LOS ANGELES, CALIFORNIA

1 SSTRE  
1 SSTRE - MAJ BREWINGTON  
1 SSZID  
1 SSTRG - LT COL LEVIN  
1 SSTSW

BALLISTIC SYSTEMS DIVISION  
NORTON AF BASE, CALIFORNIA

1 BSVDA - CAPT W. H. BLACK  
1 BSVDA - CAPT P. T. BAKER

RESEARCH & TECHNOLOGY DIVISION  
DOLLING AF BASE  
WASHINGTON 25, DC

1 RTNW  
2 TECHNICAL LIBRARY

ARNOLD ENGINEERING DEVELOPMENT CENTER  
ARNOLD AF STATION, TENNESSEE

1 AETV - MAJ BROWN  
2 TECHNICAL LIBRARY

ELECTRONIC SYSTEMS DIVISION  
L. G. HANSCOM FIELD  
BEDFORD, MASSACHUSETTS

1 ESAT

ROME AIR DEVELOPMENT CENTER  
GRIFFISS AF BASE, NEW YORK

1 RAALD

AF CAMBRIDGE RESEARCH LABORATORIES  
L. G. HANSCOM FIELD  
BEDFORD, MASSACHUSETTS

1 CRXL

AF WEAPONS LABORATORY  
KIRTLAND AFB, NEW MEXICO

1 WLAX  
2 WLL  
1 WLRPT/CAPT GILLESPIE  
1 WLRPD



1	AF MISSILE TEST CENTER PATRICK AFB, FLORIDA MTSAT
1	AF FLIGHT TEST CENTER EDWARDS AF BASE, CALIFORNIA FTOOT
1	AIR UNIVERSITY MAXWELL AFB, ALABAMA AUL-9764
1	STRATEGIC AIR COMMAND OFFUT AFB, NEBRASKA SAC(OA)
2	OFFICE OF NAVAL RESEARCH WASHINGTON 25, DC PHYSICS DIVISION
1	US NAVAL ORDNANCE LABORATORY CORONA, CALIFORNIA
1	US NAVAL WEAPONS LABORATORY DAHLGREN, VIRGINIA
1	US NAVAL WEAPONS EVALUATION FACILITY KIRTLAND AFB, NEW MEXICO
1	US NAVAL ORDNANCE LABORATORY SILVER SPRING, MARYLAND
1	US NAVAL ORDNANCE TEST STATION CHINA LAKE, CALIFORNIA
3	US NAVAL RESEARCH LABORATORY WASHINGTON 25, DC CODE 6240
2	TECHNICAL LIBRARY

2 ARMY MISSILE COMMAND  
REDSTONE ARSENAL, ALABAMA

PICATINNY ARSENAL  
DOVER, NEW JERSEY

2 TECHNICAL LIBRARY  
3 SMUPA-DW8 - MR. S. STEIN/L. M. BERLOT

BALLISTIC RESEARCH LABORATORY  
ABERDEEN PROVING GROUND, MARYLAND

1 AMXBR - DR. R. J. EICHELBERGER  
3 AMXBR-T - DR. F. E. ALLISON/DR. C. GLASS  
1 AMXBR - MR. J. J. DAILEY  
2 TECHNICAL LIBRARY

1 FRANKFORD ARSENAL  
PHILADELPHIA 37, PENNSYLVANIA

US ARMY RESEARCH OFFICE  
P.O. Box CM, DUKE STATION  
DURHAM, NORTH CAROLINA

1 CRD-AA-IP

SPRINGFIELD ARMORY  
SPRINGFIELD, MASSACHUSETTS

1 SWESP-RD - P. F. FOLEY

ARMY MATERIEL COMMAND  
WASHINGTON 25, DC

1 AMCRD-DE-W

1 FIELD COMMAND DASA (FCDR)  
SANDIA BASE  
ALBUQUERQUE, NEW MEXICO

DEPT OF THE INTERIOR  
BUREAU OF MINES  
4800 FORBES AVENUE  
PITTSBURGH 13, PENNSYLVANIA

1 R. W. WATSON

1 ATOMIC ENERGY COMMISSION  
TECHNICAL INFORMATION EXCHANGE  
P. O. Box 62  
OAKRIDGE, TENNESSEE

20 DEFENSE DOCUMENTATION CENTER  
CAMERON STATION  
ALEXANDRIA, VIRGINIA

1 NATIONAL AERONAUTICS & SPACE ADMINISTRATION (NASA)  
WASHINGTON 25, DC

LEWIS RESEARCH CENTER (NASA)  
21000 BROOKPARK ROAD  
CLEVELAND 35, OHIO

2 F. STEPKA  
1 TECHNICAL LIBRARY

2 AMES RESEARCH CENTER (NASA)  
MOFFETT FIELD, CALIFORNIA

LANGLEY RESEARCH CENTER (NASA)  
LANGLEY AFB, VIRGINIA

1 TECHNICAL LIBRARY  
1 PROTECTIVE STRUCTURE SECTION - E. KRUSZEWSKI

MARSHALL SPACE FLIGHT CENTER (NASA)  
HUNTSVILLE, ALABAMA

1 MMSAM

2 DIRECTOR, USAF PROJECT RAND  
VIA: AF LIAISON OFFICE  
1700 MAIN STREET  
SANTA MONICA, CALIFORNIA

AEROSPACE CORPORATION  
P. O. Box 95085  
LOS ANGELES, CALIFORNIA

2 DR J BROWN  
2 MR C KELLEY  
1 MR R FARRIN  
1 MR V FROST  
2 TECHNICAL LIBRARY

1	AEROSPACE CORPORATION
2	SAN BERNADINO, CALIFORNIA
	MR. D. SINGER
	TECHNICAL LIBRARY
3	AEROJET-GENERAL CORPORATION
	ATTN: K N KREYENHAGEN
	11711 S WOODRUFF AVE
	DOWNEY, CALIFORNIA
3	ARO, INC
	ATTN: VKF-AB, J PAYNE
	ARNOLD AFS, TENNESSEE
6	THE BOEING COMPANY
	ATTN: J F LUNDEBURG/R ELAM
	7755 E MARGINAL WAY
	SEATTLE, WASHINGTON
2	BATTELLE MEMORIAL INSTITUTE
	ATTN: BATTELLE-DEFENDER
	505 KING AVE
	COLUMBUS, OHIO
1	COLUMBIA UNIVERSITY
	ELEC RSCH LAB, ATTN: MR W KONIG
	632 W 125TH ST
	NEW YORK 17, NY
1	FALCON R&D
	ATTN: A M KRILL
	1567 MARION ST
	DENVER 18, COLORADO
1	GENERAL ELECTRIC CO
	ATTN: MR G ASHLEY
	LAKESIDE AVE
	BURLINGTON, VERMONT
2	GENERAL MOTORS CORP
	ATTN: J W GEHRING
	6767 HOLLISTER AVE
	GOLETA, CALIFORNIA

- 1 GENERAL DYNAMICS/POMONA  
ATTN: C BONK  
1675 W 5TH ST  
POMONA, CALIFORNIA
- 3 ILLINOIS INST OF TECH RSCH INST  
ATTN: F ZIMMERMAN  
10 W 35TH ST  
CHICAGO 16, ILLINOIS
- 1 MB ASSOCIATES  
ATTN: DR A BIEHL  
PO Box 196  
SAN RAMON, CALIFORNIA
- 1 THE MARTIN COMPANY  
ATTN: (TECH LIB, MR W R PORTER)  
SAND LAKE ROAD  
ORLANDO, FLORIDA
- 1 NORTHROP - NORTRONICS, INC  
ATTN: (B KARIN)  
500 E ORANGETHORPE  
ANAHEIM, CALIFORNIA
- 1 RAYTHEON COMPANY  
ATTN: MSL SYS DIV, W HURD  
BEDFORD, MASS
- 1 STANFORD RSCH INST  
ATTN: MR J CROSBY  
MENLO PARK, CALIFORNIA
- 1 INST OF SCIENCE & TECHNOLOGY  
UNIVERSITY OF MICHIGAN, ATTN: BAMIRAC LIB  
WILLOW RUN AIRPORT  
YPSILANTI, MICHIGAN
- 5 NAVAL RESEARCH LABORATORY  
CODE 6240  
WASHINGTON 25, DC

2 FOR: GENERAL ELECTRIC Co, MSVD  
ATTN: D E NESTLER  
3198 CHESTNUT ST  
PHILADELPHIA, PA

1 AVCO CORP, RAD  
ATTN: M ROCKAWITZ  
201 LOWELL ST  
WILMINGTON, MASS

1 SHOCK HYDRODYNAMICS, INC  
ATTN: R J BJORK  
2444 WILSHIRE BLVD  
SANTA MONICA, CALIF

AIR PROVING GROUND CENTER (PGWRT)  
EGLIN AFB, FLA

1 FOR: HAYES INTERNATIONAL CORP  
ATTN: DR C M ASKEY  
BIRMINGHAM, ALA

1 GENERAL ELECTRIC COMPANY  
ATTN: DR T D RINEY  
SPACE SCIENCES LABORATORY  
KING OF PRUSSIA, PA

BALLISTIC RESEARCH LABORATORIES (AMXBR-T)  
ABERDEEN PROVING GROUND, MD

1 FOR: GENERAL DYNAMICS CORP  
GENERAL ATOMIC DIVISION  
ATTN: M WALSH  
SAN DIEGO, CALIF

FIELD COMMAND DASA (FCDR)  
SANDIA BASE

1 ALBUQUERQUE, NEW MEXICO  
FOR: PHYSICS INTERNATIONAL  
ATTN: J HARLAN  
2229 FOURTH ST  
BERKELEY 10, CALIF

2 DEFENSE ATOMIC SUPPORT AGENCY  
ATTN: DOC LIB BR  
WASH 25, DC

1 ARMY WEAPONS COMMAND  
ATTN: AMSWE-RDW/F. W. AHRENS  
ROCK ISLAND ARSENAL, ILLINOIS

2 GENERAL ATOMIC DIVISION  
GENERAL DYNAMICS CORPORATION  
ATTN: TECH INFO SERVICES  
PO Box 5, OLD SAN DIEGO STN  
SAN DIEGO, CALIF

2 SCIENTIFIC & TECHNICAL INFO FAC  
ATTN: NASA REP (SAK/DL)  
PO Box 5700  
BETHESDA, MARYLAND

1 LOCKHEED AIRCRAFT CORPORATION  
M&S DIVISION  
TECHNICAL INFORMATION CENTER  
3251 HANOVER ST  
PALO ALTO, CALIF

DETACHMENT 4 ASD (ASQTR)  
EGLIN AFB, FLORIDA  
FOR:

1 UTAH R&D COMPANY  
ATTN: DR. E. CANNON  
1820 S INDUSTRIAL ROAD  
SALT LAKE CITY, UTAH

AIR PROVING GROUND CENTER  
EGLIN AFB, FLORIDA

1 PGF  
2 PGAPI  
1 PGWR

DETACHMENT 4 ASD  
EGLIN AFB, FLORIDA

1 ASQ  
1 ASQTR  
20 ASQWR

**UNCLASSIFIED**

**UNCLASSIFIED**